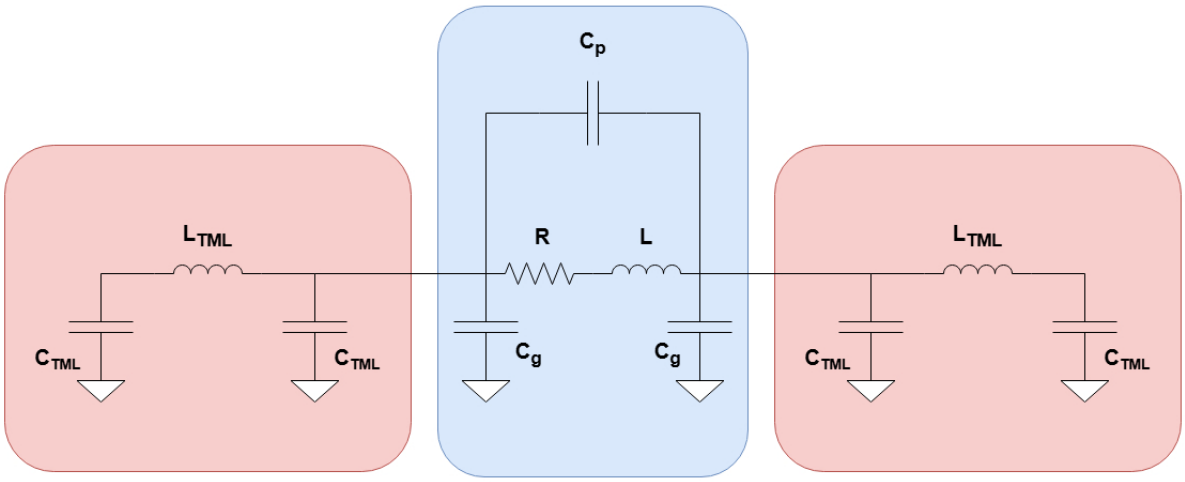

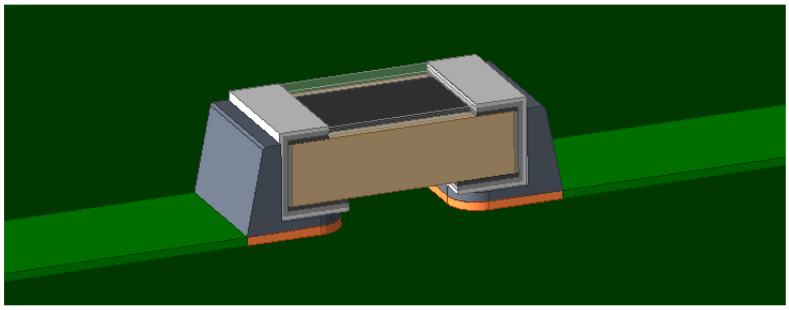

High frequency modeling of SMD resistors

Creating 3D and equivalent circuit models to capture the parasitics of SMD resistors up to 42 GHz

Master's thesis in Wireless Photonics & Space Engineering

JOHN ANDERSSON, MALIK FAHD

Department of Microtechnology and Nanoscience
CHALMERS UNIVERSITY OF TECHNOLOGY
Gothenburg, Sweden 2024
www.chalmers.se

Master's thesis 2024

High frequency modeling of SMD resistors

Creating models to capture the parasitics of SMD resistors up to 42 GHz

John Andersson
Malik Fahd

CHALMERS
UNIVERSITY OF TECHNOLOGY

Department of Microtechnology and Nanoscience

Microwave Electronics Laboratory
Chalmers University of Technology
Gothenburg, Sweden 2024

High frequency modeling of SMD resistors
Creating 3D and equivalent circuit models to capture the parasitics of SMD resistors up to 42 GHz
John Andersson
Malik Fahd

Supervisor: Per Gustavsson, Ericsson
Examiner: Dan Kuylenstierna, Microwave Electronics, Microtechnology and Nanoscience

Master's Thesis 2024
Department of Microtechnology and Nanoscience
Division of Microwave Electronics Laboratory
Chalmers University of Technology
SE-412 96 Gothenburg
Telephone +46 31 772 1000

Cover: Wind visualization constructed in Matlab showing a surface of constant wind speed along with streamlines of the flow.

Typeset in LaTeX
Printed by Chalmers Reproservice
Gothenburg, Sweden 2024

High frequency modeling of SMD resistors

Creating 3D and equivalent circuit models to capture the parasitics of SMD resistors up to 42 GH

John Andersson, Malik Fahd
Department of Microtechnology and Nanoscience
Chalmers University of Technology

Abstract

Passive components, including resistors, capacitors, and inductors, are fundamental in electrical circuit design. Surface mount devices (SMDs) are extensively used in microwave hardware development at high frequencies and precise simulations of SMD components are crucial. This thesis highlights the unpredictability of SMD resistors and underscores the importance of accurate simulations for achieving expected performance and creates a 3D and equivalent circuit models of 0402 and 0201 SMD resistors to do this. 3D models are created and verified using real measurements of a SMD resistor up to 32 GHz, while the target is for the model to be valid in 42 GHz. This model is used to create an equivalent circuit model and a scalable model for ADS that can scale the substrate height, relative permittivity and the resistance of the resistor which can be used when developing microwave circuits such as attenuators. The film that is the resistive element of the SMD component is shown to be the biggest contributing factor to parasitics. The thickness and width of the film were studied, and it was concluded that the width affected the parasitics the most. Results show very good agreement between 3D model and real measurement as well as agreement between equivalent circuit models and 3D models. The scalability ranges between 0-500 Ohm with relative permittivity being adjustable between 2.6-5 and 4.7-13 Mil substrate height. Through optimization using the scalable model, a T-attenuator is created and compared with a 3D simulation which shows very good agreement in S_{11} with less agreement in S_{21} in terms of a small frequency shift. The methods of this thesis can be extended to creating models of SMD inductors and conductors.

Keywords: 3D modeling, Equivalent circuit modeling, Scalable models, passive components, SMD resistors, high-frequency applications, parasitic effects, HFSS, ADS

Acknowledgements

The authors would like to express their gratitude to the Ericsson team for their invaluable assistance and guidance throughout this project, as well as for providing the necessary resources that made this work possible. Thanks to Tobias Wegeland and Per Gustafson for their excellent supervising, and to Ahmed Hassona, Olle Axelsson, Stefan Thöresson, Henrik Felding and Jens Fredriksson for their support in the development of the modeling and the physical measurements concerning microwave and RF-related topics. Lastly, we would like to thank our examiner Dan Kuylenstierna for following the work from the start, giving excellent guidelines and helping with theoretically related topics.

John Andersson & Malik Fahd, Gothenburg, June 2024

Contents

List of Figures

List of Tables

1

Introduction

Passive components, including resistors, capacitors, and inductors, play a fundamental role in electrical design. In particular, surface mount devices (SMDs) find extensive use in printed circuit board (PCB) circuits for radio frequency (RF) applications. These components serve diverse purposes, such as circuit stabilization, amplifier biasing and impedance matching between different stages in transmitters. As hardware development increasingly relies on circuit and electromagnetic simulations, ensuring the reliability of these simulations becomes critical. This paper discusses the challenges associated with passive SMD resistors at microwave frequencies, emphasizing the need for accurate simulations to align realized product performance with expected behavior.

At lower frequencies, the prediction of circuit behavior is typically intuitive. However, when dealing with microwave frequencies, a host of challenges emerges. These challenges includes contributions from parasitic effects. Of particular significance are passive SMDs, whose characteristics undergo substantial changes at high frequencies as is shown in this thesis. As a consequence, the simplistic models commonly employed become inadequate for describing their behavior accurately.

1.1 Purpose

This research project aims to advance the understanding and modeling of SMD resistor components, with a specific focus on resistors within the 50-100 Ohm range and in the size of 0201 and 0402 see table 2.1 for exact dimensions. Operating in the frequency range of 0-42 GHz, these components play a critical role in modern high-frequency electronic systems. Unlike traditional resistor performance metrics such as heat tolerance and power handling, The primary objective is to accurately characterize the parasitic effects that introduce reactance as the frequency varies.

The proposed models will encompass both equation-based equivalent circuits and three-dimensional geometrical representations. The equation-based model will be designed for scalability, accommodating variations in resistance, substrate height, and substrate permittivity. By achieving accurate modeling, we aim to enhance the reliability of circuit simulations and contribute to the optimization of high-frequency electronic designs.

1.2 Background

In this section, the project background is presented to give the reader an insight into the importance of accurate modelling and provide reasoning behind the complexities involved in high frequency modelling. Previously reported resistor modellings from research articles and industry will initially be presented.

1.2.1 Project background

In the realm of equivalent circuit models, both corporate entities and independent researchers have contributed valuable insights. For instance, Vishay proposes an equivalent circuit model specifically tailored for thin film resistors [1], spanning the frequency range from 0.1 to 40 GHz. This model serves as a foundational tool for understanding the frequency response of such resistors. Additionally, inspired by this approach, researchers have developed equivalent circuit models of lumped elements [12], based on measurements conducted within the 0.5 to 5 GHz frequency span on microstrips. The procedure differs from this work as their models are based on measurements, whereas this project relies on EM simulations for circuit modeling. The advantages of both methods will be discussed later.
When it comes to 3D models of resistors, the available information is scarce. Modelithics, in their discussions , emphasize the significance of 3D simulations in high-frequency design to mitigate unnecessary costs [7].

This research initiative represents a collaborative effort with Ericsson, a global leader in networking and telecommunications. Ericsson leverages models from an external company specializing in RF measurement-based component modeling, employing them as a licensing service. The validity of these models extends from 0 to 10 GHz or up to 20 GHz, contingent upon the specific resistor manufacturer. However, beyond these frequencies, the extrapolation of model values has been demonstrated to yield inaccuracies, particularly when approaching millimeter-wave (mm-wave) frequencies. However, this project's model will be based on resistors from a specific manufacturer. This project targets frequencies exceeding 40 GHz, increasing the challenge.

Parasitic effects pose significant challenges in the design of microwave components, particularly in the context of attenuators. Attenuators play a crucial role in signal conditioning, allowing precise control over signal power levels. However, when employed in up-converted signals for example, practical issues arise specifically, deviations between simulated and actual attenuation values. Consider the example of a T-attenuator. During design and subsequent board production, the simulated attenuation often diverges considerably from measured values. This discrepancy primarily stems from parasitic reactance induced by component geometry and environmental factors. As the frequency increases, these parasitic effects become increasingly pronounced, causing the resistor to exhibit reactive behavior which is discussed in 2.1.3. To address this challenge, microwave designers must capture and account for these parasitic effects. Various compensation techniques can be employed, tailored to the

specific application. Our research project aims to develop comprehensive circuit and 3D models that accurately represent component behavior up to 42 GHz. By doing so, this project also seek to enhance the reliability of high-frequency designs and facilitate efficient attenuation optimization.

In existing electronic circuits, specialized SMD components with high precision at microwave frequencies are commonly employed to mitigate parasitic effects. However, these precision components come at a considerable cost, often reaching several dollars per unit. In contrast, standard SMD components are significantly more affordable, priced at a fraction of the cost. This pragmatic approach presents a straightforward solution to address the issue. Hardware costs play a pivotal role in overall cost calculations, and for companies like Ericsson, which engage in large-scale production of RF modules, implementing this approach could yield substantial cost savings.

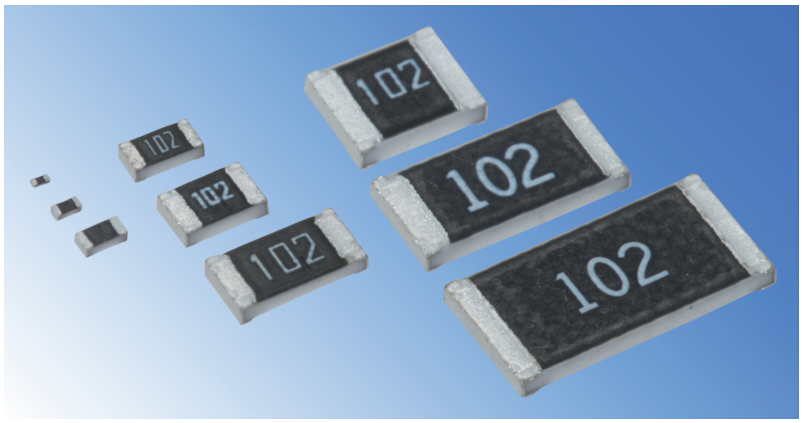

Figure 1.1: Image of several different sizes of SMD resistors. Image courtesy of KOA Corporation, further sharing of image outside of thesis is forbidden as requested by KOA corporation.

2
Theory

2.1 Fundamentals of SMD passive components and individual parts that make up a resistor

This section describes and discuss the theory regarding SMD passive components. The composition of a SMD resistor is shown and the individual parts are defined, later part of the theory section is about parasitics and what the cause behind them is and how the expected behaviour of a resistor on the Smith chart is affected as the frequency and consequently the parasitics increases. Finally the discussion regarding the 3D model and theory behind the equivalent circuit model will be introduced.

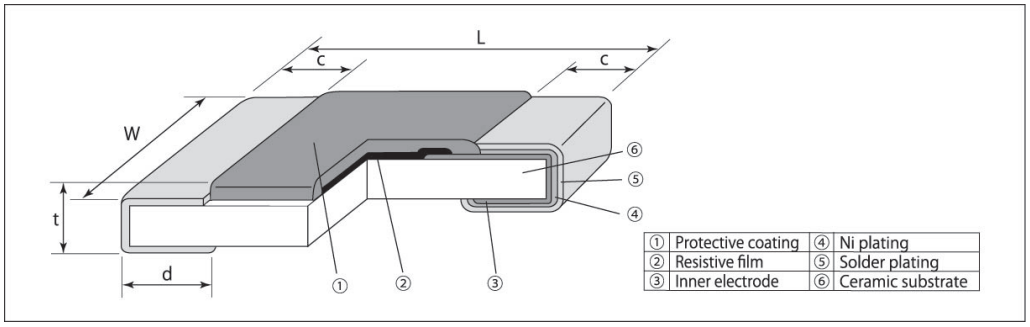

Figure 2.1: Provided image in a datasheet of a SMD resistor. Note the three layered termination, image courtesy of KOA Corporation. Further sharing of image outside of thesis is forbidden as requested by KOA corporation.

2.1.1 Passive components & resistors

The resistor is a component that is used to create a stable current flow throughout a circuit, it may also be used to reduce or divide voltage. An application can be the creation of a T-attenuator that would make use of three SMD resistors in a configuration to achieve a desired attenuation. Another application would be a resistor on a bias line to a transistor or right before a transistor for stabilization. Passive components can be designed as an SMD component that are suitable for dimension-wise small applications such as RF applications. SMD size ranges from 0.4mm x 0.2 mm as the smallest to 7.4mm x 5.1 mm as the largest. To remember these different sizes, they have been associated with chip package types. The smallest 0.4mm x 0.2mm is called a 01005 while the largest is called 2920. See table 2.1 for some but not all sizes.

Chip package type	Dimensions (mm)
01005	0.4 x 0.2
015015	0.38 x 0.38
0201	0.6 x 0.3
0402	1.0 x 0.5
0603	1.5 x 0.8
1210	3.2 x 2.5

Table 2.1: Different sizes of SMD components and their associated chip package type.

2.1.2 Composition of a SMD resistor

SMD resistors utilize thin or thick film technology as seen as (2) in figure 2.1, each offering distinct advantages based on their application in terms of frequency and power handling. Thin film resistors exhibit lower parasitic inductance and capacitance, making them well-suited for higher-frequency applications [8][2]. Conversely, thick film resistors excel in power handling and provide a broader range of resistance values. The thickness difference between these two film types can be substantial, sometimes exceeding a factor of 1000.

A fundamental SMD resistor comprises four essential elements, often composed of various materials to achieve desired properties.

- A substrate
- Resistive element
- Terminal
- Coating

The substrate material, commonly alumina-based or ceramic, plays a critical role. Selection depends on specific properties such as thermal handling capabilities. The resistive element, typically an alloy, bridges the two ends of the SMD component. Commonly used metals include nickel and chromium. The terminal facilitates electrical connection to the circuit. The terminal's design may be of several layers or single layered see (3) and (4) in figure 2.1. The coating protects the resistor from environmental factors and mechanical stress. The overall resistance of an SMD resistor primarily hinges on the resistive element, which can be accurately determined using equation 2.1.

$$R = \frac{\rho L}{A} \tag{2.1}$$

Where $\rho = \frac{1}{\sigma}$ is the resistivity of the material with the conductivity σ being the inverse of ρ, L is the length of the material and A is the cross sectional area. By rearranging terms, a desired resistivity can be calculated in order to achieve a resistance of the SMD component with a certain film size. This is explained in the method section to pre-determine the resistance value of a 3D model of a resistor in Ansys.

2.1.3 Parasitics in a SMD resistor

An ideal resistor, when represented on a Smith chart, would consistently occupy a single point along the real gamma axis, regardless of frequency. The precise location of this point depends on the reference impedance Z_0 and the load impedance Z_L. The load impedance comprises both a real part (resistance) and an imaginary part (reactance). Refer to Table 2.2 for a comprehensive list of elements and their associated resistance/reactance characteristics.
At lower frequencies, the impact of reactance—such as that introduced by parasitic effects from transmission lines—remains negligible. However, as frequency increases, this effect becomes more pronounced. The specific shift of the point as caused by a reactance load depends on the dominant parasitic at that frequency range. For instance, an inductive reactance in series would shift the point upward and to the right, tracing along a constant resistance circle.
Figure 2.2 illustrates the parasitics arising from the composition of an SMD resistor. On a transmission line, capacitive reactance emerges due to the space between the conductor and the ground plane. Within this region lies the substrate, which significantly influences the relative permittivity ε_r. The effects of varying ε_r on transmission line parasitics are well-documented by Pozar here [3]. Additionally, a difference in voltage across the two resistor terminals introduces another capacitance (depicted as the capacitor on the blue substrate in the figure 2.2).
Metals within the resistor contribute to inductive parasitics due to self-inductance. Self-inductance arises from the current flowing through the metal, generating a magnetic field and associated magnetic flux. As this flux changes with current variations, Lenz's law dictates the introduction of self-inductance, see [11] for a more detailed explanation.

Element	**Impedance**
R	$Z_L = \mathrm{R}$
L	$Z_L = \mathrm{j}\omega\mathrm{L}$
C	$Z_L = 1/\mathrm{j}\omega\mathrm{C}$

Table 2.2: List of passive elements and corresponding impedance equation.

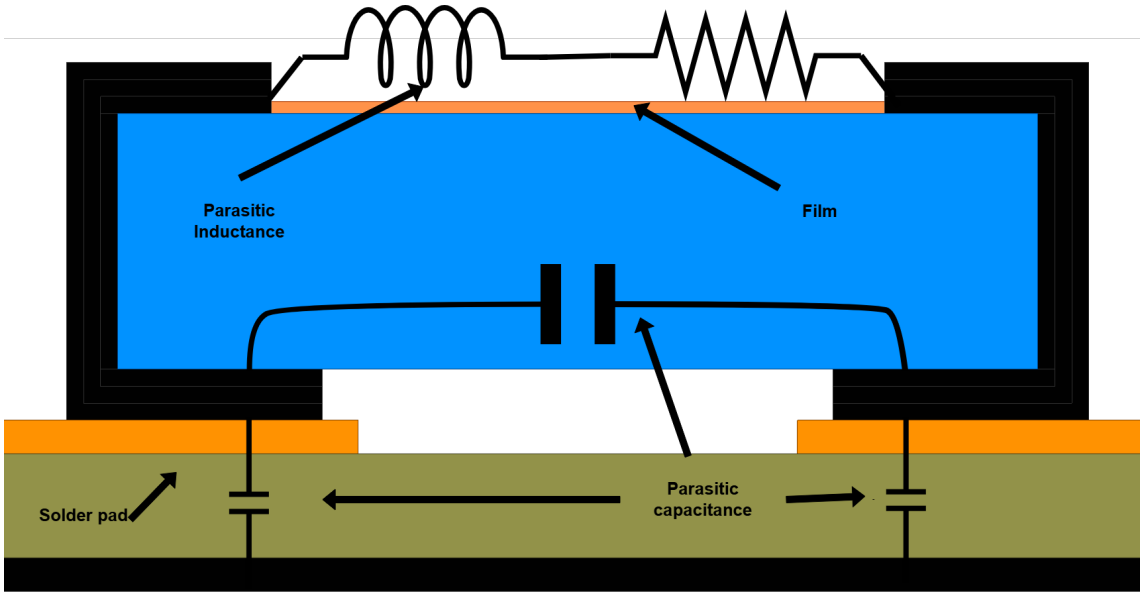

Figure 2.2: Simple 2D sketch of a SMD resistor with parasitics indicated

2.1.4 The difficulty of accurate modeling

There are two significant methods for modeling passive components: equivalent circuit models and 3D electromagnetic structures. In certain cases, these methods complement each other, as exemplified in this project.
3D Modeling:

- **Accurate Representation**: 3D modeling involves precisely depicting the composition, materials, and dimensions of the specific passive component. When the structure is faithfully replicated, this method stands out as the most accurate. It accounts for effects such as shielding, coupling, and interactions with the environment.
- **Complexity and Accuracy**: By capturing intricate details, 3D modeling provides a comprehensive understanding of the component's behavior. However, it demands computational resources and expertise in full wave EM simualation tools or other numerical techniques.

Circuit Modeling:

- **Equation-Based Approach**: Circuit modeling relies on equations and simplifies the design process. Design engineers find it more accessible due to its reduced simulation time.
- **Scalability and Optimization**: With scalability, adjusting various configurations—such as substrate properties, resistor values, and solder pad dimensions—becomes as straightforward as pressing a button. Consequently, optimization efforts are streamlined.

The challenge lies in accurately translating all contributing factors from a 3D structure into a circuit schematic. As frequency increases, even subtle contributions become significant. Designers must carefully account for parasitics and and factors that might affect the reliability of the results.

Extracting the values for an equivalent circuit eventually requires an S-parameter file, obtained either through real measurements with a Vector Network Analyzer (VNA) or from an EM simulation featuring accurately constructed components. In any case, the equivalent circuit model is unable to accommodate effects like shielding, coupling, and interactions with components and lines. Typically, a microwave designer begins by simulating at the circuit level and concludes with 3D simulations to validate circuit performance and lastly adjust/tune parameters. This design approach is effective, as it allows relatively fast attainment of desired results with scalable models, followed by verifying EM simulations with minimal iterations. It is therefore important to include both variants in the modelling. Referring to the previous example of the T-attenuator, one can efficiently optimize various configuration types to quickly achieve the desired attenuation through a well made scalable circuit model which can be verified with a 3D simulation.

The largest uncertainties lies within the 3D models as they require accurately depicting the composition, materials, and dimensions of the specific passive component. If the structure is correctly replicated, this is by far the most accurate method as it accounts for effects such as shielding, coupling and interactions with the environment. However, the composition of passive SMD components are IP (Intellectual property), this limit the publicly available information regarding materials and dimensions which is necessary for accuracy. In this sense the publicly available information found online is small and the topic unexplored. A SMD 50 Ohm resistor from two different manufacturers will to the naked eye look almost identical with the rectangle body and two terminations on each side see figure 1.1 and **??**. These might however have very different performance due to e.g. different internal structure, dimensions and materials of the resistive film and metal termination, see figure 2.1 for an example of this. Simply looking at these resistors will not reveal anything except for the dimensions of the body.

Due to the ambiguity that comes from competition between manufacturers with their IP, only speculations can be made regarding what is contributing to these parasitics which is what we are looking to capture in our 3D models to accurately predict how a resistor will behave. To verify or deny speculations, several simulations will be performed to rule out what is and is not a deciding factor in the performance of a resistor. A deciding factor in this context is a factor that deviates the results significantly.

2.2 Equivalent Circuit Model

A SMD resistor can be considered a π-network as shown in figure 2.3 (b). Expanding on this general network, the EC model is made to include the capacitance C_p which, when the resistor is divided in to two symmetrical halves, represents the capacitance due to the voltage difference across the two resistor ports. C_g are capacitances that occur because of the conductor and the ground plane on each side of the substrate as seen in figure 2.2. C_g is assumed to be the same on both sides of the resistor, this assumptions is further explored in subsection 2.2.1 but is nevertheless valid in a 3D simulation that is made to be symmetric. The Y-parameter matrix of this circuit can be seen in 2.2.

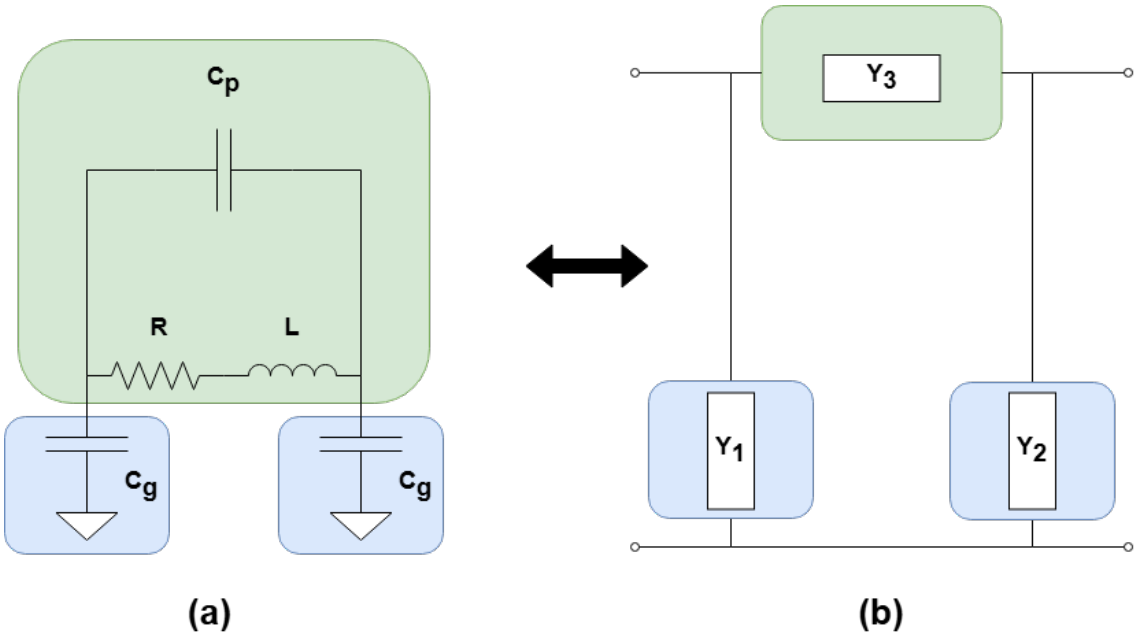

Figure 2.3: (a) Simple π-network representation of the 3D model resistor, (b) A general π-network. Colored boxes are used to clarify what part in (b) represents the same part in (a) but expanded on.

$$Y = \begin{bmatrix} jwC_p + \frac{1}{R+jwL} + j\omega C_g & -(\frac{1}{R+jwL} + jwC_p) \\ -(\frac{1}{R+jwL} + jwC_p) & jwC_p + \frac{1}{R+jwL} + j\omega C_g \end{bmatrix} \tag{2.2}$$

The imaginary and real part of the matrix elements are separated to achieve the following matrix.

$$Y = \begin{bmatrix} \frac{R}{R^2+w^2L^2} - j\omega(C_p + C_g + \frac{L}{R^2+\omega^2L^2}) & \frac{-R}{R^2+w^2L^2} + j\omega(\frac{L}{R^2+\omega^2L^2} - C_p) \\ \frac{-R}{R^2+w^2L^2} + j\omega(\frac{L}{R^2+\omega^2L^2} - C_p) & \frac{R}{R^2+w^2L^2} - j\omega(C_p + C_g + \frac{L}{R^2+\omega^2L^2}) \end{bmatrix} \tag{2.3}$$

The equations 2.7 -2.9 can then be used to extract the corresponding component values. See section 2.2.2.2 for the extracted equations. If R is unknown it can be calculated from S-parameters using equation 2.4.

$$R = 50 \cdot \frac{1 + S(1,1)}{1 - S(1,1)} \tag{2.4}$$

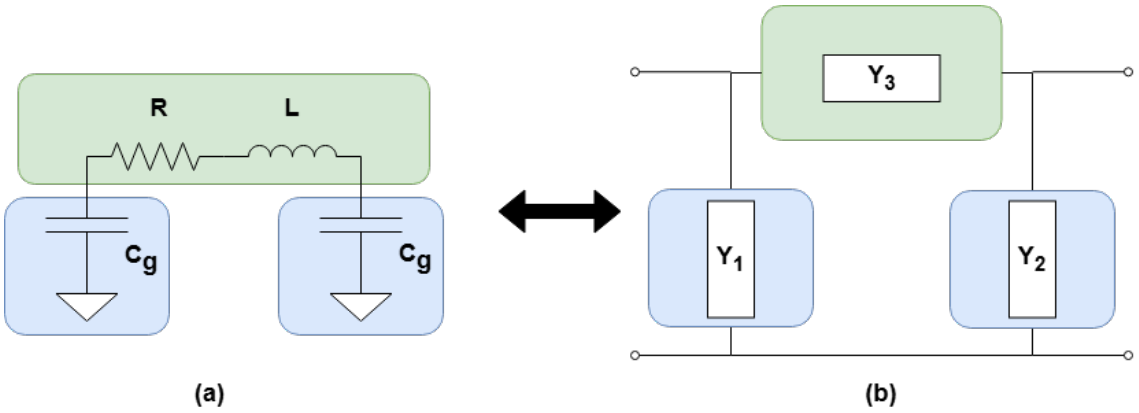

Figure 2.4: (a) Simple π-network representation of the 3D model resistor without C_p, (b) A general π-network.

This model in lower frequency will represent a resistor well which will be shown in the result section. When the frequency increases this model is no longer adequate because the parasitics due to the solder pads will start to have a notable contribution to the reactance as is shown in the model comparison in the result section.

Another model can be seen in figure 2.4. This model omits the shunt capacitor C_p and is a model that proposed in the paper here [12] published by IEEE. The values of C_g, R and L will for this method be calculated through different means. This other method distinguishes C_g which the previous model does not.
By keeping Y_1 and Y_2 separate and treating them individually, one can calculate these through the use of S-parameters or ABCD-parameters. See the following equations 2.10 - 2.12
When this is done one can look at the imaginary part or the reactance of Z_1 to Z_3 after a Y to Z conversion to identify if the reactance are inductive or capacitive. This will reveal if the reactance of both capacitors to ground are equal or not and can hence improve the accuracy. Testing this method on S-parameters gathered from a 3D simulation shows that the quotient of the reactance between these two capacitors when measuring a 0201 resistor is very small. The down-side of this method is that C_p and L are indistinguishable i.e. Information is lost because the total reactance of Y_3 is considered. This will not affect results at low frequencies but as the frequency increases the contributing parasitic C_p may increase and hence inaccuracy increases due to C_p not being considered in the model. A clear impact while testing is that the S_{21} parameter showed less losses than what was simulated using a 3D model, including C_p resolves this issue which is shown in the result section.

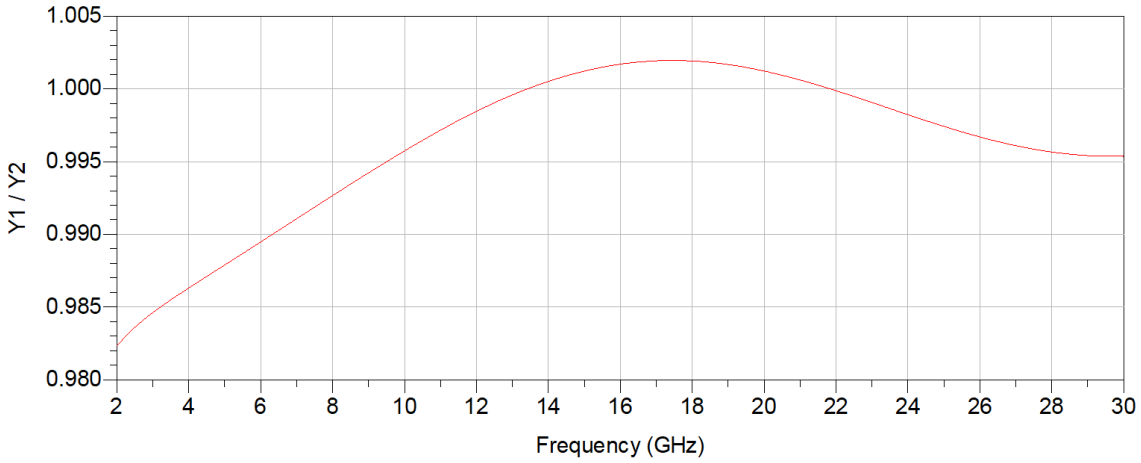

Figure 2.5: Quotient of the inverse reactance of Y_1 and Y_2. Measured using a 0201 3D model. A difference can be observed although it is very small.

The difference in accuracy between the two models will be presented in the result section and then discussed further.

2.2.1 Improving the equivalent circuit model

Solder pads are small exposed transmission lines where the SMD component will be soldered onto, see figure 2.6.
By including transmission lines in the EC model, effects associated with transmission lines such as loss and parasitics can be accounted for which will yield better accuracy. This will be shown in the result section.

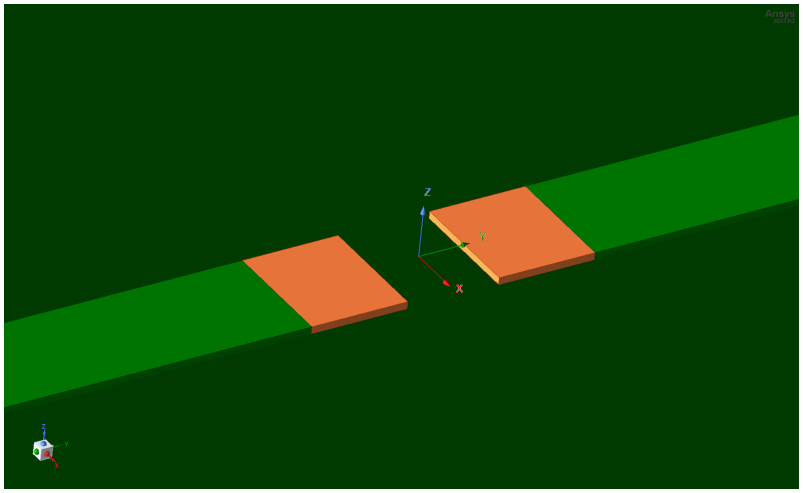

Figure 2.6: An image of a PCB created in Ansys with Co-planar waveguide as transmission line. A part of it is highlighted as orange to show the exposed part of the transmission line also called the solder pad where the resistor is soldered on.

In Figure 2.7 a second order π network is presented. This model introduces transmission lines that are approximated as the inductor L_{TML} and further improved with

the addition of capacitors C_{TML}, this addition of capacitors improves the bandwidth of which this approximation is valid. Note that this approximation is valid for electrically short transmission lines. This is due to a Taylor approximation that is used to simplify with the condition that $\beta l << 1$ where βl is the electrical length. See Appendix A.1 for the derivation of this approximation.

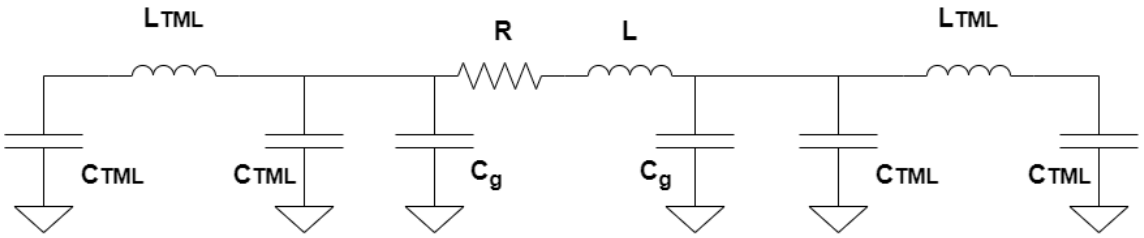

Figure 2.7: Second order π network representation of the KOA resistor. Note the two new π networks on the sides that are approximations of a transmission line. This was applied to both models that was earlier presented. This figure only shows one of the models.

2.2.2 Extracting parameters

The parameters can be categorized into two distinct groups: intrinsic parameters and extrinsic parameters. In this context, intrinsic parameters refer to those associated with the internal characteristics of a system, while extrinsic parameters pertain to external factors. Refer to Figure 2.8 for further clarification.
Within the red and blue boxes in the figure, these parameters can be independently extracted from each other. Alternatively, a more complex approach involves combining the ABCD matrices of three individual networks. However, this results in a 2x2 matrix containing eight unknowns, or six if C_{tml} and C_g can be considered equal due to symmetry. Instead of pursuing this intricate method, the option of separately extracting these parameters was explored. Remarkably, this approach demonstrated improved accuracy, as evidenced in Figure 4.12.

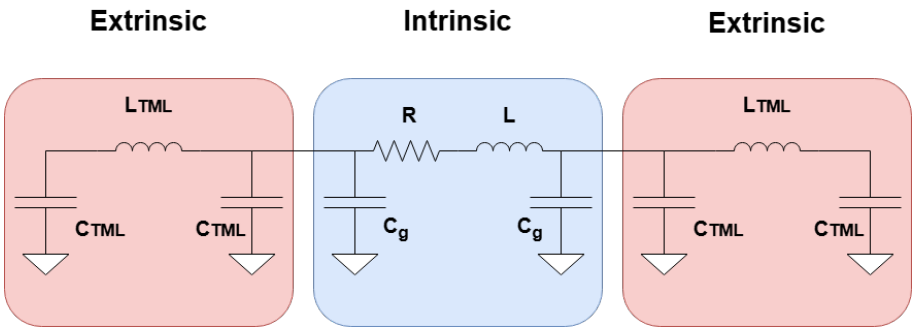

Figure 2.8: Second order π-network representation of a resistor with indicated extrinsic and intrinsic parts of the model.

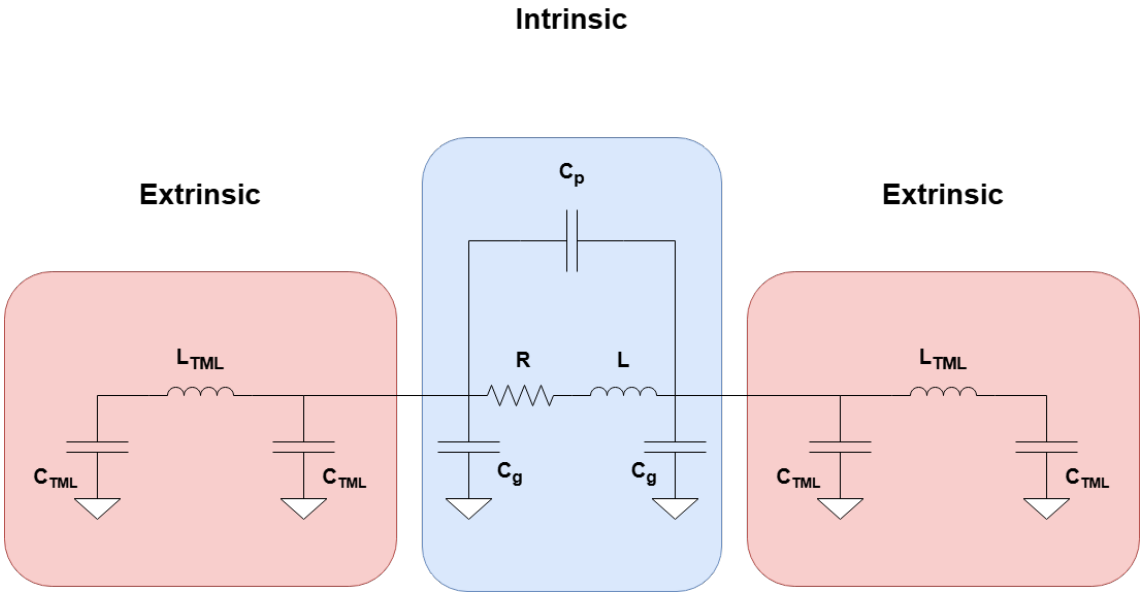

Figure 2.9: Second order π-network representation of a resistor with indicated extrinsic and intrinsic parts of the models.

2.2.2.1 Extrinsic Parameters

The extrinsic parameters are shown in equation 2.5 and 2.6.

$$L_{TML} = \frac{Z_0 \beta l}{\omega} \tag{2.5}$$

$$C_{TML} = \frac{\beta l}{2\omega Z_0} \tag{2.6}$$

Where Z_0 represents the characteristic impedance of the microstrip, and βl corresponds to the electrical length. Specifically, β denotes the imaginary part of the propagation constant, also known as the phase constant, while l represents the physical length of the microstrip. Additionally, ω stands for the angular frequency.
Notably, these extrinsic parameters can be extracted independently from the intrinsic part, which is the resistor itself. This property allows for the inclusion of scalable parameters in the model. For instance, consider the solder pads to which this resistor would be attached. By treating them as separate entities, it avoids the need for extensive matrix algebra when incorporating transmission lines. Consequently, this approach streamlines the analysis process.

2.2.2.2 Intrinsic parameters

The intrinsic parameters include the ones in the blue box in figure 2.8 of the first model and 2.9 for the second model. For the first model, these were derived from the matrix seen in equation 2.3 and shown in equation 2.7 - **??**. Note that there is no equation for R which is intentional. The value R is pre-determined. If it is unknown it can easily be extracted from the $S(1,1)$ value at DC using equation 2.4. Note that if a resistor is simulated in a two port and the second port has a certain impedance, it is necessary to remove this impedance from the calculation of R as $S(1,1)$ will include this quantity. As an example, if the second port is 50 Ohm and the resistor itself is 50 ohm then the Smith chart will show the resistor at DC having a value of 100 ohm.

$$L = \sqrt{\frac{R}{Re(Y_{11})} - R^2} \cdot \frac{1}{w} \tag{2.7}$$

$$C_p = \frac{L}{R^2 + (wL)^2} - \frac{Im(Y_{12})}{w} \tag{2.8}$$

$$C_g = \frac{Im(Y_{11})}{w} - C_p + \frac{L}{R^2 + (wL)^2} \tag{2.9}$$

For the second model the equations are, as derived in the article [12]

$$Y_1 = \frac{D-1}{B} \tag{2.10}$$

$$Y_2 = \frac{A-1}{B} \tag{2.11}$$

$$Y_3 = \frac{1}{B} \tag{2.12}$$

Where A,B,C,D are ABCD-parameters that can be calculated using S-parameters. When Y_1 - Y_3 are calculated they will need to be identified as capacitive or inductive depending on the negative or positive susceptance and if they are in shunt or in series.

3

Methods: How to create reliable models

This section will introduce the methods with the purpose to construct accurate models for frequencies reaching up to 42 GHz. The approach for obtaining 3D, equivalent circuit, and scalable equivalent circuit models will be explained and discussed in detail.

3.1 3D EM Simulations

3.1.1 HFSS Setup

It is well known that 3D EM simulations are the most accurate tool for microwave computer simulations. However, that is only true if the simulation represents a reality based environment with good meshing, excitation and analysis setup. Figure 3.1 illustrates the simulation environment designed for simplicity to minimize the need for fine meshing, resulting in quicker simulations. The table below the figure consists of pad dimensions as well as substrate properties.

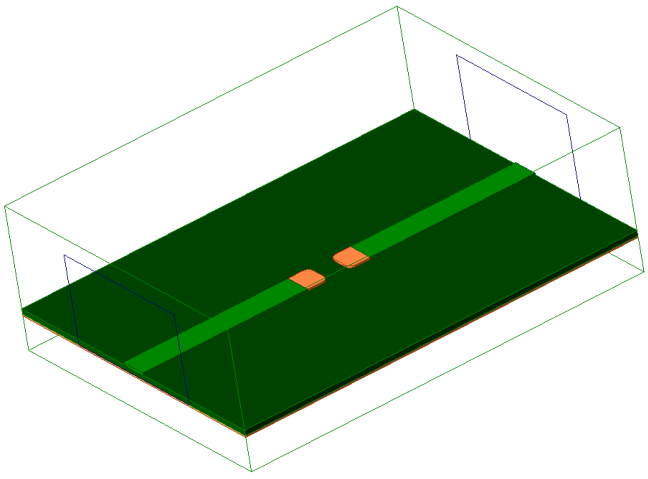

Figure 3.1: 3D Environment on which the 3D model of a resistor is placed. The dark green part is the substrate with a ground plane conductor placed underneath (orange) and a microstrip conductor above (light green). The exposed orange metal parts are the solder pads. An airbox can be observed with a size that yields accurate and quick simulations with wave ports placed on each side.

0402 / 0201 (All dimensions in mm)		
Pad length	**Pad gap**	**Pad width**
0.42 / 0.31	0.44 / 0.3	0.53 / 0.33
Port width & length	H_{sub}	ε_r
6 x Pad width 10 x Pad length	0.1016	3.66

Table 3.1: Dimensions of crucial parameters required to recreate the simulation environment. Note that absence of a "/" sign imply that both 0402 and 0201 share the given dimension.

The pads are designed according to Ericsson standards and since they use the same dimensions, it is therefore not of interest to create models that are scalable with pad size. The port size was chosen within the Ansys recommendations interval [13] and some investigations. It was found that the dimensions in the table was suitable as they yielded convergence to the correct port impedance and avoided excitation of unwanted modes.

3.1.2 Modelling the resistor in general

The challenge in modeling resistors lies in the limited information provided by manufacturers regarding materials and dimensions. Typically, only exterior dimensions are disclosed, i.e. what one can see with the naked eye, while details about the interior, such as the resistive film, are lacking.
The first part of the modelling is therefore to model the resistor with all the information that is given from the datasheet and for the unknown parameters, reasonable assumptions will initially be made and later their dimensions will be varied with several steps in order to understand what parameters actually affects the performance. If an unknown parameter is crucial for the parasitic effect, then this dimension must somehow be known or at least reasonably assumed.
Achieving a resistance of 50 ohm for instance can involve various combinations of material resistivity, width, length, and thickness according to equation 2.1. Assume that the 50 ohm resistor have some specified known dimensions, by doubling the thickness and halving the width, the resistance should in theory remain 50 ohm. The production techniques employed by manufacturers to achieve desired resistances are undisclosed. However, techniques such as x-ray analysis or comparing measured resistors with 3D models provides insights into these parameters.
The main unknowns are the width and thickness of the resistive film, while the length can be assumed to be the distance between the two terminals since it needs ohmic contact. A 50 ohm resistor will be created with different width and thickness combinations in order to understand what parameter actually affects the parasitics of the component. Exploring different materials and soldering geometries is also crucial.

In this project, only a 50 Ohm resistor was available for measurement and three different resistors was x-rayed.

3.1.2.1 Modelling the resistor in detail

The image in 3.2 shows the soldering from an Ericsson board with a 0603 component, the solder thickness between the metal trace and the component are usually the same regardless if it is a 0603 or 0402 component as intended by Ericsson.

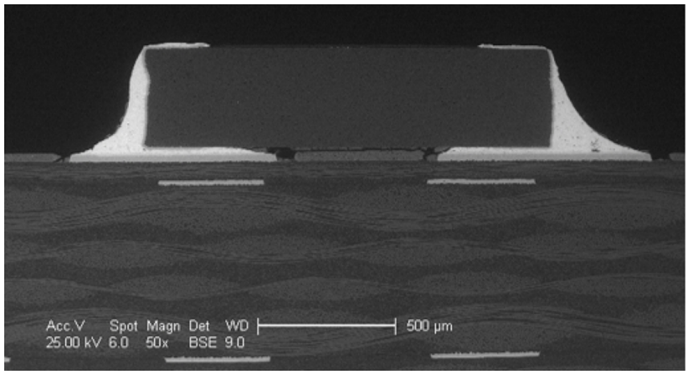

Figure 3.2: Cross section of a 0603 resistor with the solder structure clearly represented [14]

Three different SMD resistors with different sizes and resistances were x-rayed. These resistors are not from the same manufacturer as the one being modelled, however it can still provide some insight om the film dimension. From figure 3.3 the film width can be seen as well as some cuts in the film which are most likely made to trim the resistance to the exact value due to imperfect precision from the manufacturing. From the images it can be measured that the film width occupies 67%, 75% and 59% respectively from the leftmost to rightmost resistor.

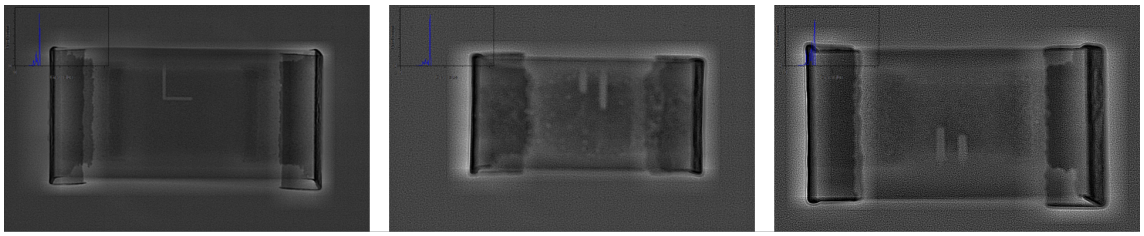

Figure 3.3: X-ray of three different SMD resistors. (a) 499 Ohm, size 1206. (b) 82 Ohm, size 0402, (c) 18 Ohm, size 0603. [14]

After carefully considering the datasheet, material information from **X (koa)** and x-ray images from Ericsson, the following 3D structure could be designed (motivation of resistive film dimensions will be explained in depth in the results and discussion).

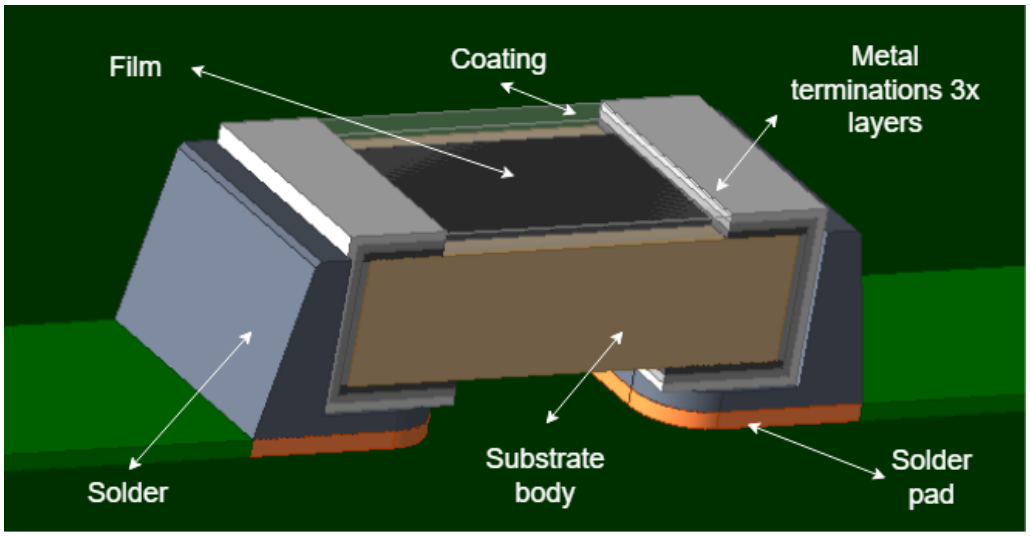

Figure 3.4: Cross section of a 0603 resistor with the solder structure clearly represented

3.2 Measurements with Ikaros board

Using a test board, a TRL (Through-Reflect-Line) calibration was performed to achieve accurate de-embedding. A similar environment to the test board was then replicated in Ansys, which involved matching the number of layers, their dimensions, and the relative permittivity (ε_r) of the substrates that form the coplanar waveguide of the board. The length of the coplanar waveguide is designed to be $\lambda/2$ at 35 GHz, meaning that at this frequency and at 0 GHz, the line is a multiple of λ. In these cases, calibration does not work due to the transmission line's length being significantly smaller than the wavelength, causing the transmission line's effects to be disregarded. Consequently, the frequency sweep was limited to the range of 2-35 GHz, with the results expected to be least accurate at the upper and lower bounds of this range.

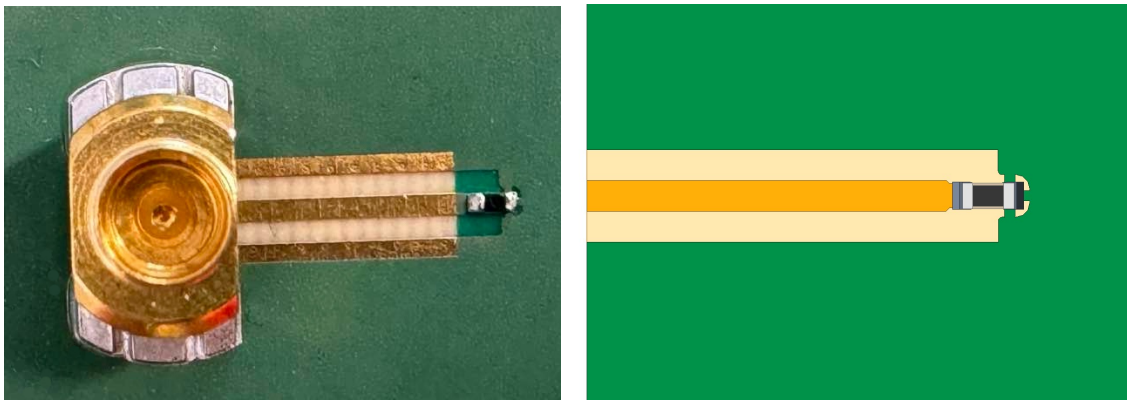

(a) (b)

Figure 3.5: (a) Ikaros board with a 47 Ohm Resistor mounted and connected to ground. (b) 3-Layer HFSS setup of the Ikaros board

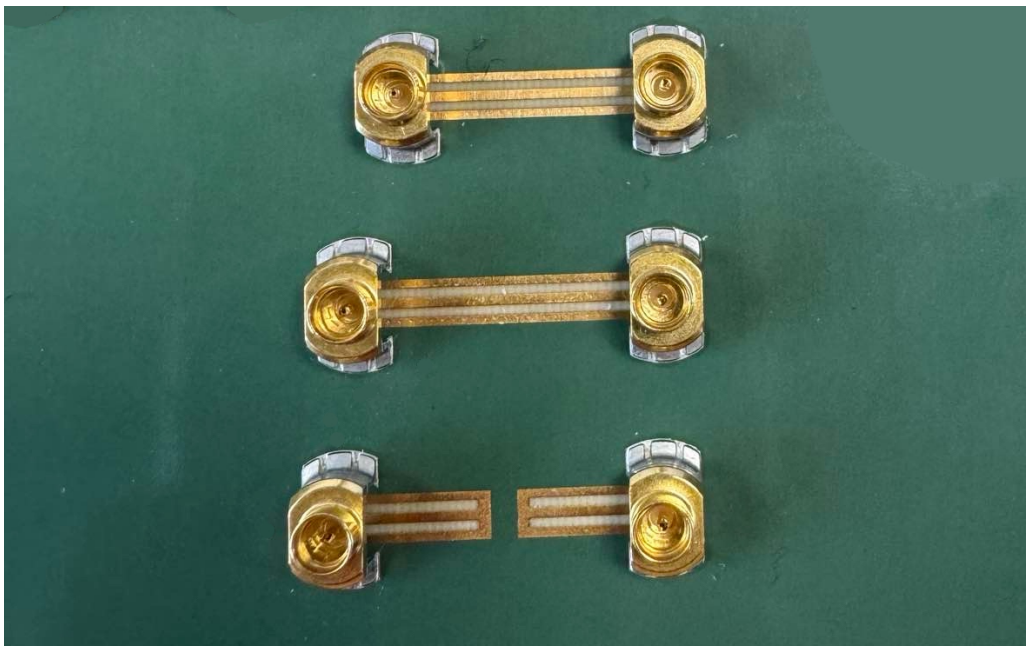

Figure 3.6: Through, line and short respectively on test board, used for TRL calibration.

3.3 Equivalent circuit model

In this section, an equivalent circuit model for SMD resistors is presented which is developed to capture the vital parasitic effects of mm-wave frequencies. The topology relies on the circuits shown in figure 2.2, consisting of two separate derivations. For the intrinsic part, the derivation was made using simple circuit analysis combined with mathematical simplifications. The extrinsic parameters which makes up the contribution for the transmission line was derived using transmission line theory, taylor approximations and ABCD matrices, explained in detail in Appendix A. However, the sophisticated methodology in this project is not so straightforward as

running a single simulation, evaluating the parameters from the equations and expect a good result. One has to carefully consider two separate de-embeds, otherwise the input values to the equations will result in a poor agreement when the values are used in a equivalent circuit model. This is further explained in the following two sections.

3.3.1 Extracting intrinsic parasitics from S-parameter files

The first step is to extract the intrinsic parameters, which is the parasitics of the resistor. Initially, the de-embedding was made from the beginning of the resistor to the end of it (orange arrows in figure 3.7). This method gave good results around 0-18 GHz but started to deviate more in the mm-wave frequencies.

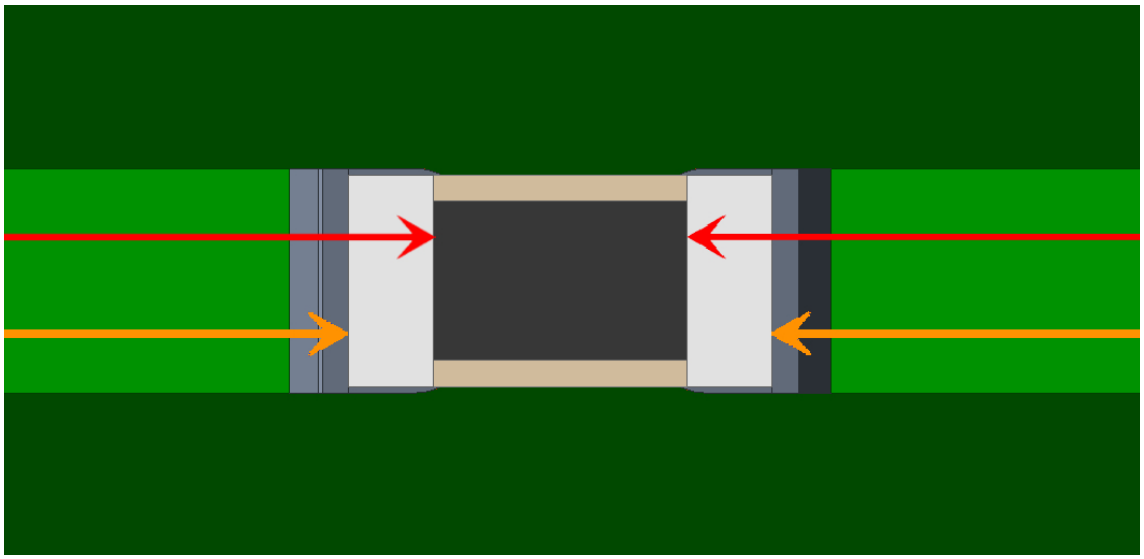

Figure 3.7: Orange: Initial de-embedding, from the ports to the metal terminations. Red: Corrected de-embedding, from the port to the resistive film. [14]

It was later found that although the the metal terminations are short, they behave as transmission lines. The higher the frequency the longer the line looks from an EM-wave perspective. At lower frequencies the contribution can therefore be considered negligible. Since the intrinsic circuit model consists of a π-network with only lumped elements, it is more reasonable to de-embed all the way to the film, excluding the transmission lines contribution which is instead a part of the extrinsic model. By employing this method, a simulation can be conducted following the red arrows, resulting in S parameters that can be converted to Y parameters. The Resistance value is then found from equation 2.4, or in simple terms by observing the DC-value of R. Finally, all variables and constants can be identified in equations 2.7-2.9, making it possible to extract C_g, C_p, and L with high accuracy. It will be shown that these three variables are slightly frequency dependent, meaning one should choose the most optimal point before parameter extraction. Choosing the parameters at 42 GHz was found to be an excellent point, yielding highly precise results between 0-42 GHz and even beyond that, which will be further discussed.

3.3.2 Extracting extrinsic parasitics from S-parameter files

The next step is to extract the extrinsic parameters of the two π-networks, denoted as C_{tml} and L_{tml}, from equations 2.5-2.6. These parameters stem from the solder pads, which, as mentioned, functions as very short transmission lines.
Note that the metal terminations were intentionally excluded from the intrinsic de-embedding to be included in the extrinsic model instead. Hence, the transmission line's actual length encompasses not just the solder pad but also the metal terminations. Considering the presence of solder, the most precise measurement method was found when assuming the effective length of transmission line to be the closest measured distance between the solder pad's start and the metal termination's end, l_1+l_2, as depicted in figure 3.8.

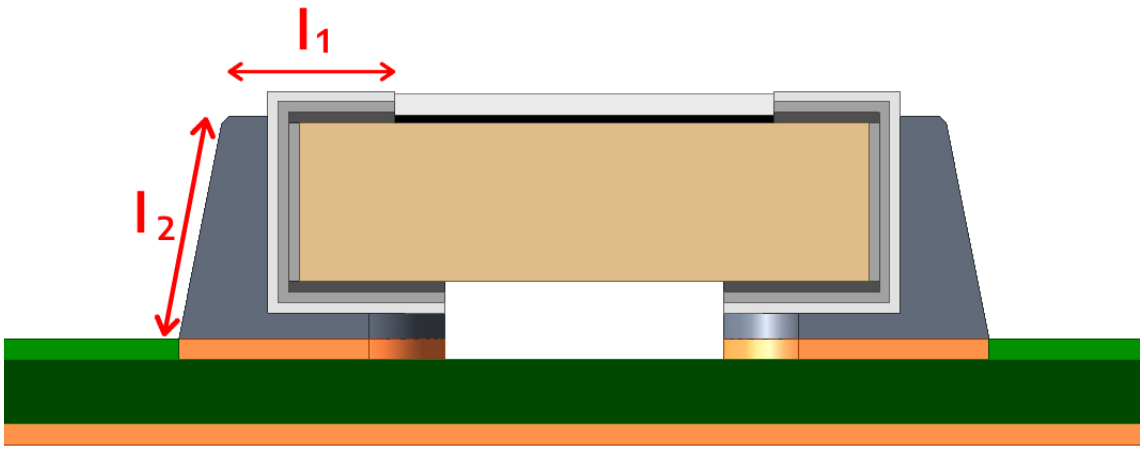

Figure 3.8: Length of transmission line used to extract extrinsic parameters [14]

By inserting the length $l = l_1$+l_2 in equations 2.5-2.6, the parasitic impedances C_{TML} and L_{TML} can be calculated. The derivation of these equations were based on a Taylor approximation, assuming that the factor $\beta l << 1$. since the factor is inversely proportional to the frequency, it is expected to be invalid at some point. Figure 3.9 shows that the factor is almost 1/2 and 1 at 42 GHz and 75 GHz respectively. The factor 1/2 was proven to be sufficient enough for a very accurate model in contrast to a factor 1 where it deviates, the exact accuracy will be shown in the results.

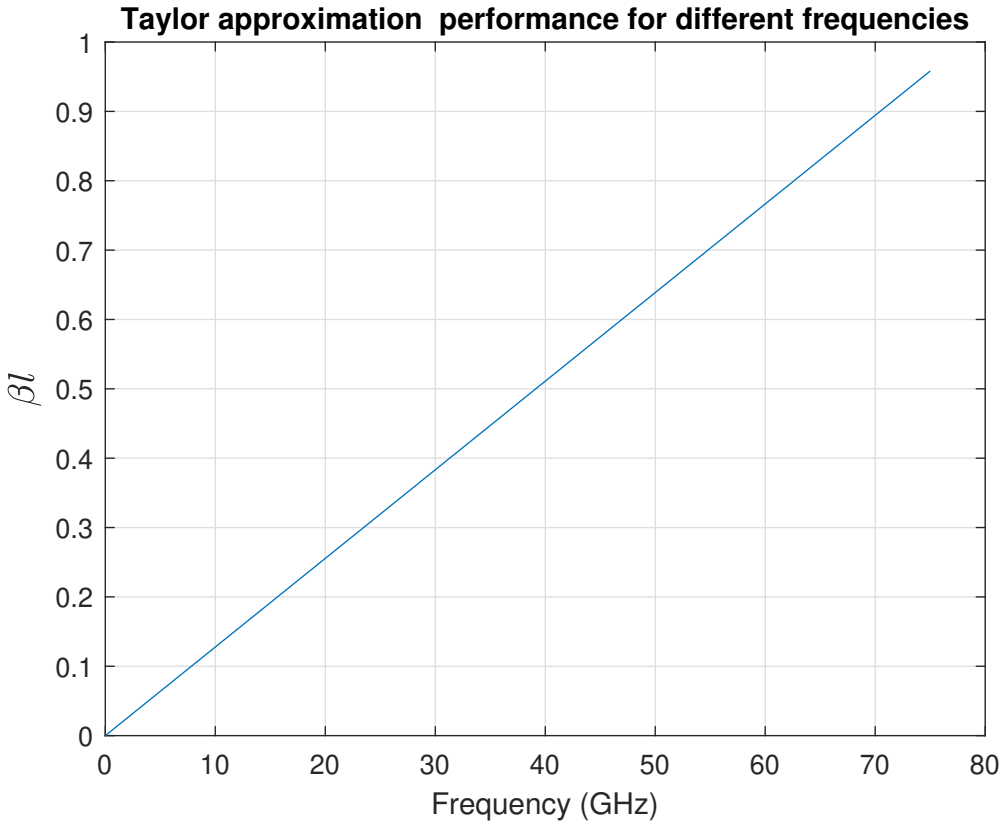

Figure 3.9: Figure shows the value of βl and how it increases with the frequency which makes the approximation used for transmission lines less valid at higher frequencies.

Finally, when all parameters have been calculated in the entire equivalent circuit, the model can be finalized and compared to the 3D simulation (or real measurement if that is what one bases their S-data on). The de-embedding must now extend to the solder pads to account for the all the parasitics, as depicted in figure 3.10.
After exporting the S-parameters from the 3D resistor model with this de-embedding, it becomes possible to plot the results against the equivalent-circuit model and conduct an analysis of the validity of the models. If certain parameter calculations are slightly inaccurate, but the overall circuit topology is correct, it should be feasible to adjust and optimize the parasitic components to improve the alignment with the models. However, more on that will be discussed in the following sections.

3.4 Creating a scalable equivalent circuit model

A scalable equivalent circuit model allows users to adjust specific parameters within a defined range where the model is considered accurate. It also allows users to input optimization goals to quickly obtain desired results, as all analysis and equations have already been pre-integrated into the scalable component which the user do not

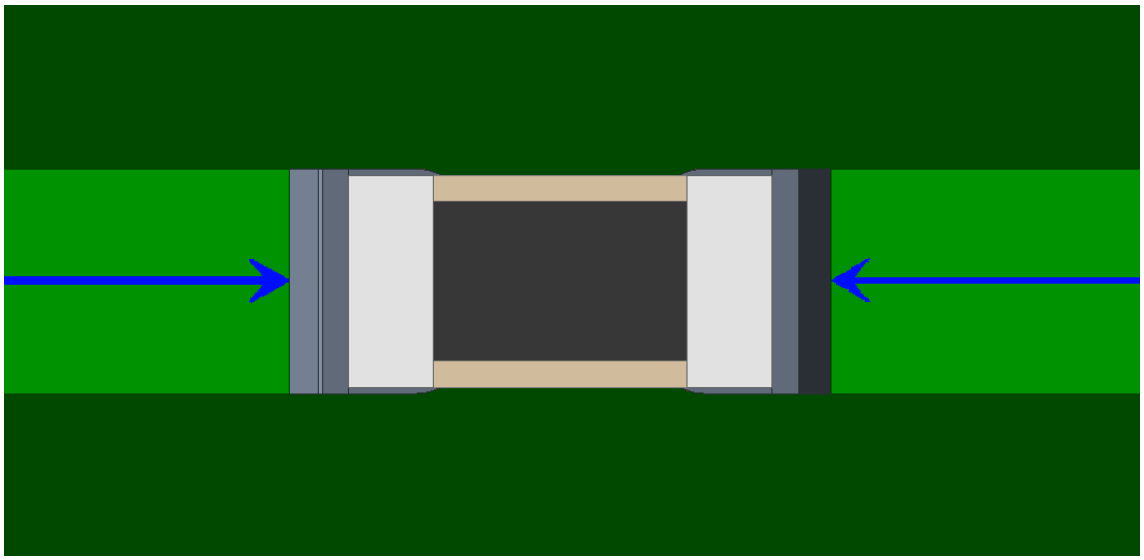

Figure 3.10: Length of transmission line used to extract extrinsic parameters [14]

need to concern about. However, values outside the specified range is extrapolated, which decreases accuracy the further one moves from the defined interval. Extrapolated values often represent uncommon or uninteresting configurations, therefore, not much emphasis has been given in these intervals. In this section, all parameters affected by scaling will be discussed, along with the reasoning behind the "valid intervals".

3.4.1 Scaling resistance

The most critical parameter to adjust is resistance, as impedance cannot be easily predicted in advance for high frequency SMD resistors. This means that the desired impedance value must be determined through tuning and optimization, primarily by adjusting the resistance.

Initially HFSS simulations of the constructed 3D Model was performed with 7 different resistance points between 42 ohm and 112 ohm in roughly 10-ohm increments. The substrate properties remained the same for these simulations meaning that the extrinsic parameters Ctml and Ltml are constant. Intrinsic parameters were then extracted using the presented model. Within this range, no tuning was necessary, as the extracted parameters closely matched the ideal values. Above 112 ohm, the equations suggest that C_p and C_g should be negative, eventually becoming complex with higher resistance, limiting the model to below 112 ohm for this 0402 SMD resistor. Therefore, beyond 112 ohm, the parameters of the circuit had to be tuned/optimized in order to match the 3D simulation. It was also found that accuracy is improved by adding a resistor in series with C_p and C_g, "R_p" and "R_g" respectively. Performance declines gradually above 112 ohm, with the model only being accurate up to 25 GHz around 500 ohm when in fact the goal ws to develop accuracy up to 42 GHz. Below 42 ohm, accuracy also decreases as resistance approaches 0 ohm, requiring parameter optimization and added ground resistances (R_g) for improvement.

To summarize the validity, the final scaling resistance interval has been developed between 1-500 Ohm. However resistances between 0-42 Ohm has to include ground resistances R_g and resistances between 112-500 ohm needs both R_g and R_p for accuracy. For visual clarification, please refer to the circuit in figure 2.9. The model becomes less and less accurate approaching very high resistances. The only interval in which the developed intrinsic model can be employed with a 'perfectly' equation based approach, without requiring any tuning, optimization, or additional components in the proposed topology, is between 42 and 112 ohm. Within the scalable component, there will be three "if-conditions" that account for each interval. In pseudocode, it resembles something like this:

if 42 $>$ R $<$ 112, then A.
R_g=*Inactive*, R_p=*Inactive*
if R $<$ 42, then B.
R_g=*Active*, R_p=*Inactive*
if R $>$ 112, then C.
R_g=*Active*, R_p=*Active*

Where A, B and C are a set of fitting equations that connects a graph between each extracted value, interpolating in between. This is done for C_g, C_p and L respectively. In the result section, the first condition will be presented and explained more in detail. It will be shown that only C_p and L varies with resistance while C_g is unaffected.

3.4.2 Scaling substrate properties

In certain scenarios, substrate properties are preselected, while in others, they remain undecided. In the latter case, it is convenient to provide users with a degree of freedom by permitting variations in substrate properties.
As the previous section mentioned, C_p and L were affected by a resistance sweep but not C_g. This is because C_g is the capacitance between the solder pad and ground plane which is logical since it has nothing to do with the resistive film. The concept of C_g is somewhat similar to a parallel plate capacitor, without the plate symmetry. The capacitance of a parallel plate capacitor is given by:

$$C = \frac{\varepsilon_r \varepsilon_0 A}{h} \tag{3.1}$$

Where ε_r and ε_0 are the relative permittivity and permittivity of free space respectively. A is the total area between the plates and h is the distance between the plates. It is not necessary to derive an exact equation for C_g, Instead, the proportionality $C \propto \frac{\varepsilon_r}{h}$ can be exploited. This relation suggests that increasing ε_r with a factor x or decreasing the substrate height h with the same factor x, the same capacitance C should be obtained. Therefore two cases are investigated, one where the permittivity is constant and the substrate height is swept and another where the height is constant and the permittivity is swept. The sweeping ratio will be identical to investigate in what ranges the proportional relation is linear. In the

linear region, the user should be able to input any height and permittivity that has a ratio within the valid range. The following cases were simulated and extracted for linearity investigation.

Investigation of substrate properties with a fixed resistance of 50 Ω		
Case A - Constant Height (7.8 mil)	**Case B - Constant Permittivity (3)**	H_{sub} / ε_r
5.00	4.68	1.56
3.64	6.43	2.14
3.30	7.09	2.36
2.93	8.00	2.67
2.60	9.00	3.00
2.39	9.80	3.27
1.8	13.00	4.33

Table 3.2: Different simulation configurations used to investigate how substrate properties affects the model in order to create relevant fitting parameters for the scalable model.

Not only is C_g affected by the substrate properties, but C_{TML}, the capacitance between the ground and the solder pads, is also influenced. Therefore, C_g is similarly investigated as a function of permittivity and height, using the same configurations as in Table 3.2. Changing permittivity and slightly changes C_p which is the capacitance between the metal terminals. The reason for this is most likely due to the changing effective permittivity between the substrate and air which is the interface of its permittivity.

It was also observed that L_{TML} changes with substrate height but remains unaffected by permittivity. This aligns with online sources, which indicate that the inductance of a microstrip line, due to loop inductance, depends on substrate height but not permittivity. Various sources use different approximations to derive inductance as a function of height. For further reading and comparison, refer to [15], [16], and [17]. Although these sources may differ in their numerical approximations and simplifications, they consistently show that inductance depends on height, typically involving a logarithmic function.

Furthermore the film inductance is slightly affected by the permittivity sweep, but this will be shown to be less significant and barely affects the performance. Much emphasis will therefore not be put on this variable in the overall scaling function.

After investing Case A and B in table 3.2 for each parameter in the circuit topology it was found that the model can be defined as valid in the intervals: $2.6 < \varepsilon_r < 5$ and $4.68 \text{ mil} < H_{sub} < 13 \text{ mil}$. The limiting variables will be exposed in the results and later discussed. Note that the intrinsic variables were extracted from the presented model, directly from the equations while the extrinsic had to be tuned for better accuracy in higher frequencies. This is also discussed later.

4
Results

With the use of the methods presented earlier and the models that were constructed, the models can now be used for analysis. This section will presents results regarding the parasitic behaviour of the resistor models of the sizes 0402 and 0201. Results regarding the comparison between the two models that was presented in section 2.2 where two models were proposed will be shown. Further on the equivalent circuit models of the first order and second order will be compared to the EM-simulations. Finally simulations and fitted equations for the scalable model will be presented.

4.1 3D Model

As mentioned before, the analysis of the parasitic behaviour involves varying different parameters that are assumed to affect the parasitics. Among these parameters are the thickness **T** of the film and the width **W** of the film. Before the analysis, a board with a resistor of the size 0402 was used to verify the 3D model. The verification is needed to ensure that the analysis using the 3D model will reflect how a real 0402 resistor would behave. A similar board with a 0201 resistor was not available for testing.

4.1.0.1 Verifying the 3D model

The result of the VNA measurement is shown in figure 4.2 and the 3D model is shown in figure 4.1.
Using these results, it is decided that the 3D model is sufficient enough to be used for analysis. Differences on the Smith chart is credited due to uncertainties in the measurement a uncertainty here is how a TRL calibration is limited at electrical lengths 0° and 180° due to a multiple of $\frac{\lambda}{2}$ making a load at the end of a "line" look like a "through" as expected from the explanation in 3.2. This will mainly affect the measurement close to DC and at 35 GHz (a chosen upper limit). See the original paper of the proposed TRL calibration method here [5] for further explanation of how this affects the calibration.

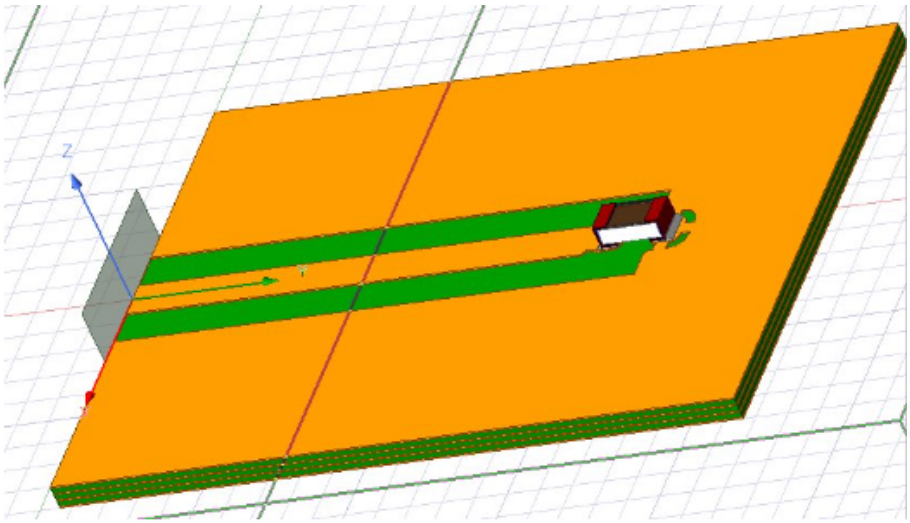

Figure 4.1: A 3D model resistor placed in the environment that was made to be like the real test-board.

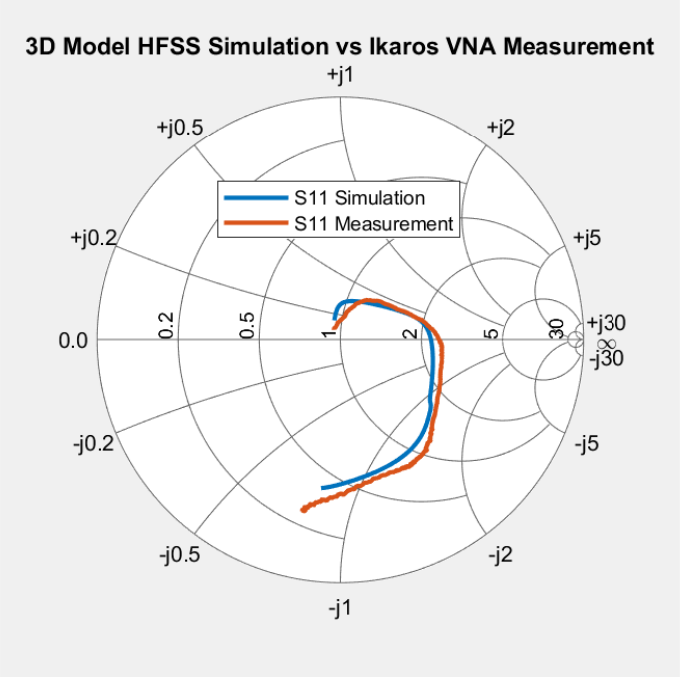

Figure 4.2: A comparison of the S_{11} parameters of the measurement performed with a 0402 resistor and the simulation of the 0402 3D model. Note that the behaviour of the real measurement is captured in the 3D simulation in terms of bends.

4.1.1 0402 film dimension comparison

As a reminder to the reader, film dimensions are varied to draw conclusion regarding how, by varying, will the parasitics be affected. The main interesting dimensions are the width and the thickness of the film.

4.1.1.1 Thickness comparison

The thickness was varied beginning with a original estimated thickness of the film called **T**. The other thicknesses were $\frac{T}{100}$, $\frac{T}{500}$, $\frac{T}{1000}$. The results of these measurements can be observed in figure 4.6 (a) & (b). The deviation in behavior in the Smith chart as frequency increases is negligible.

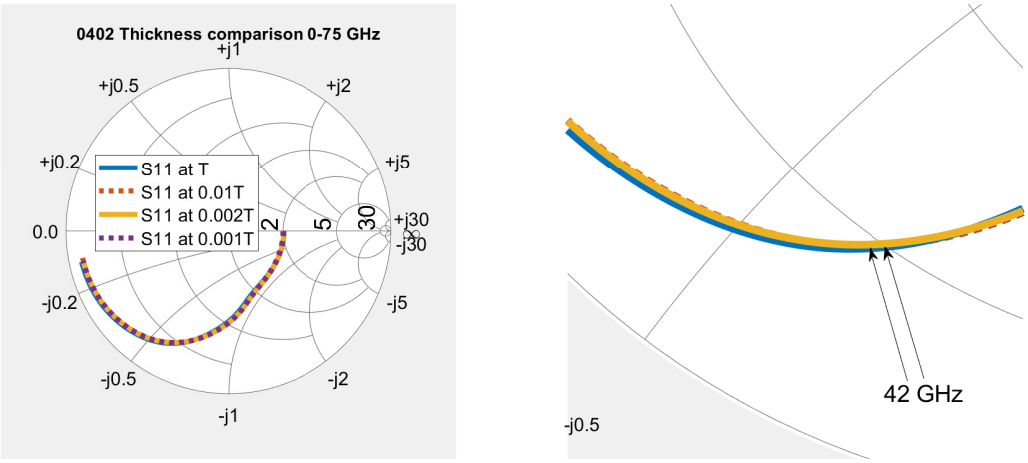

(a) (b)

Figure 4.3: (a) shows the S_{11}-parameter comparison between 4 different thickness sizes. (b) shows a zoomed in portion of (a). Note how synced the S_{11}-parameters are in (b).

4.1.1.2 Width Comparison

The width **W** of the film was varied and the comparison can be seen in figure 4.4 (a) & (b). The widths that were simulated was the original width W that covers the whole area between the terminals, $\frac{2W}{5}$, $\frac{3W}{5}$ and $\frac{4W}{5}$.

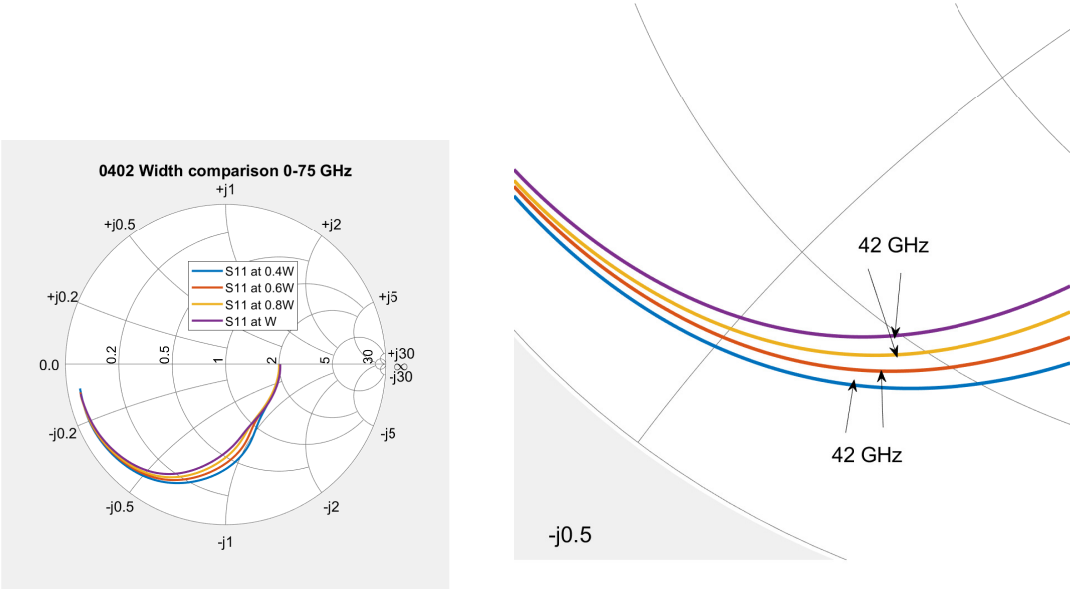

(a) (b)

Figure 4.4: (a) shows the S_{11}-parameter comparison between 4 different widths. (b) shows a zoomed in portion of (a). Similarly to the thickness comparison, these simulations are quite synced frequency wise on the Smith chart.

4.1.2 0201 film dimension comparison

4.1.2.1 Thickness comparison

The thickness was varied in the same way as it was for the 0402 thickness comparison, i.e. $\frac{T}{100}$, $\frac{T}{500}$, and $\frac{T}{1000}$.

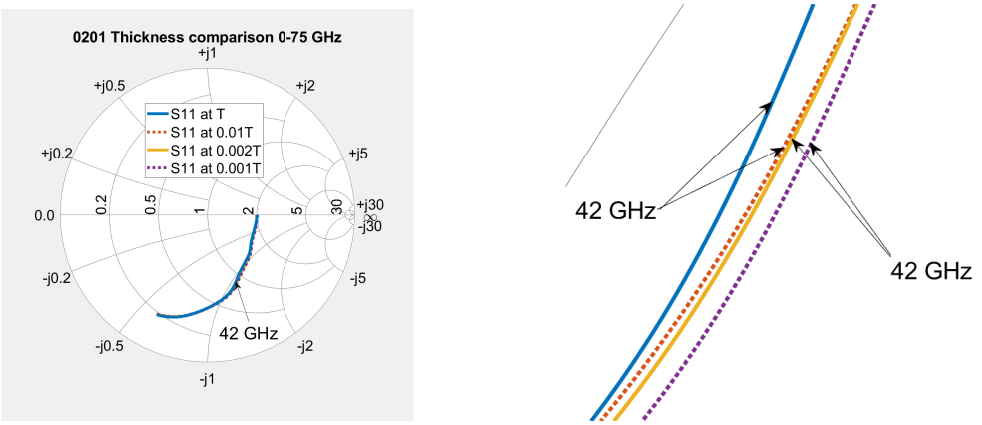

(a) (b)

Figure 4.5: (a) shows the S_{11}-parameter comparison between 4 different widths. (b) shows a zoomed in portion of (a) that shows how synced the simulations are at 25 GHz.

4.1.2.2 Width Comparison

The width was also varied in the same way as it was for the 0402 width comparison.

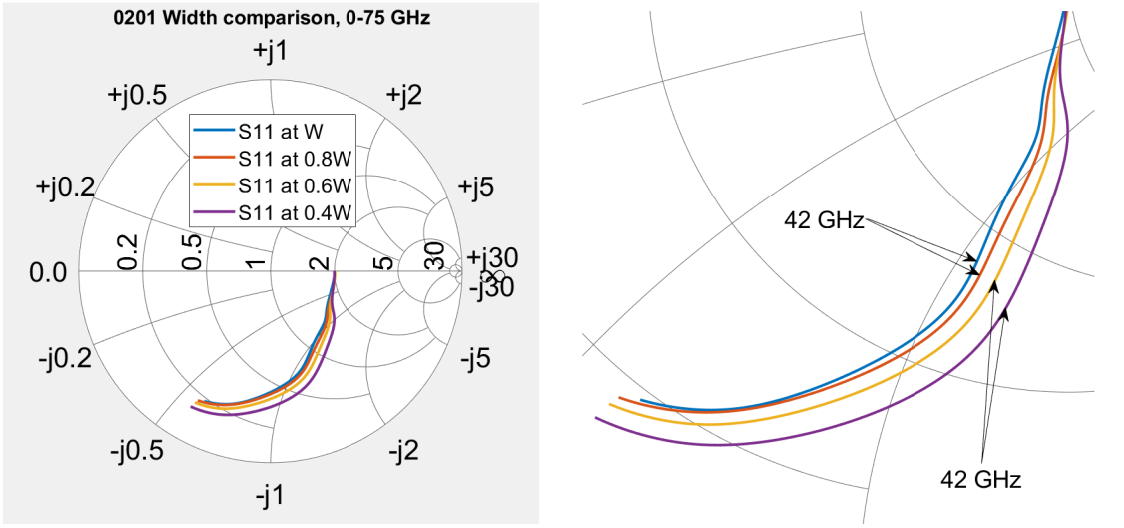

(a) (b)

Figure 4.6: (a) shows the S_{11}-parameter comparison between 4 different widths. (b) shows a zoomed in portion of (a) with the 45 GHz points highlighted.

4.2 Equivalent Circuit Model

Using the S_{11}-parameters from the 3D simulations, parameter extraction is now possible to create the equivalent circuit models. Arbitrary 0402 and 0201 50 Ohm resistors were simulated in Ansys for this purpose.

4.2.1 Extraction of parameters using the model with a shunt capacitor

4.2.1.1 0402 Parameters

Using the equations 2.7 - 2.9 that were derived from the matrix 2.3 and selecting the value of C_p, C_g, L at 42 GHz yield the following values:

$$C_p = 8.7 \text{ fF}$$
$$L = 0.35 \text{ nH}$$
$$C_g = 39 \text{ fF}$$

L_{tml} and C_{tml} was also extracted by using equation 2.5 and 2.6 respectively.

$$C_{tml} = 38 \text{ fF}$$
$$L_{tml} = 54 \text{ pH}$$

Putting these values of the lumped components in the second order equivalent circuit shown in figure 2.7 yields the results seen in figure 4.7 which compares these results with the S_{11}-parameters from the corresponding 3D simulation. (c) shows the difference in S_{11}-parameters values between the simulation and equivalent circuit model.

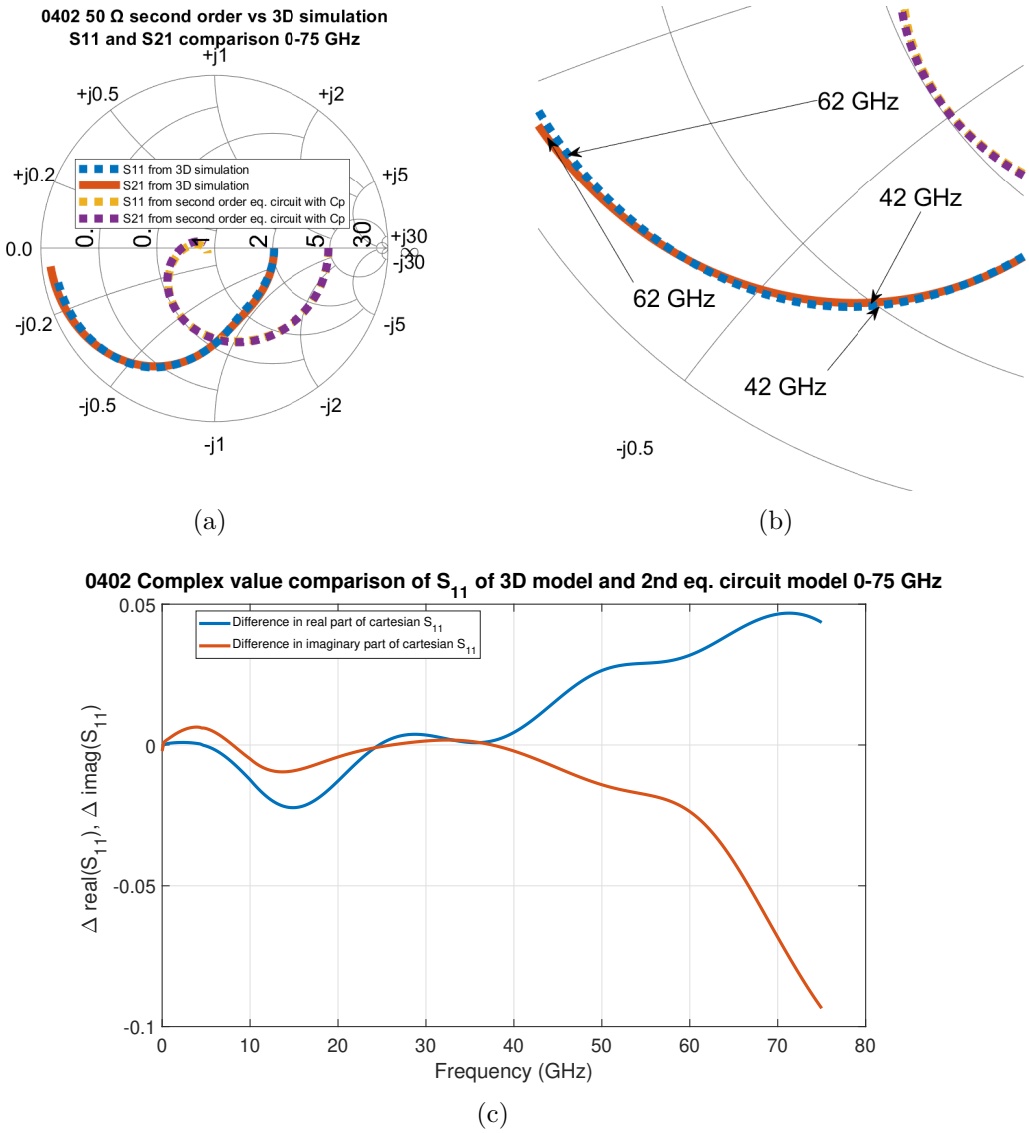

Figure 4.7: (a) A comparison of the S_{11}-parameters from a 3D simulation and a second order equivalent circuit. The S_{11}-parameters from the 3D simulation was used to extract the values of the components in the equivalent circuit. (b) zoomed in version of (a) which highlight how synced both models are at frequencies beyond 42 GHz. (c) A real and imaginary part value comparison between the two simulations.

4.2.1.2 0201 parameters

With the same procedures as for the 0402 model, the parameters were extracted and the results are shown in figure 4.8

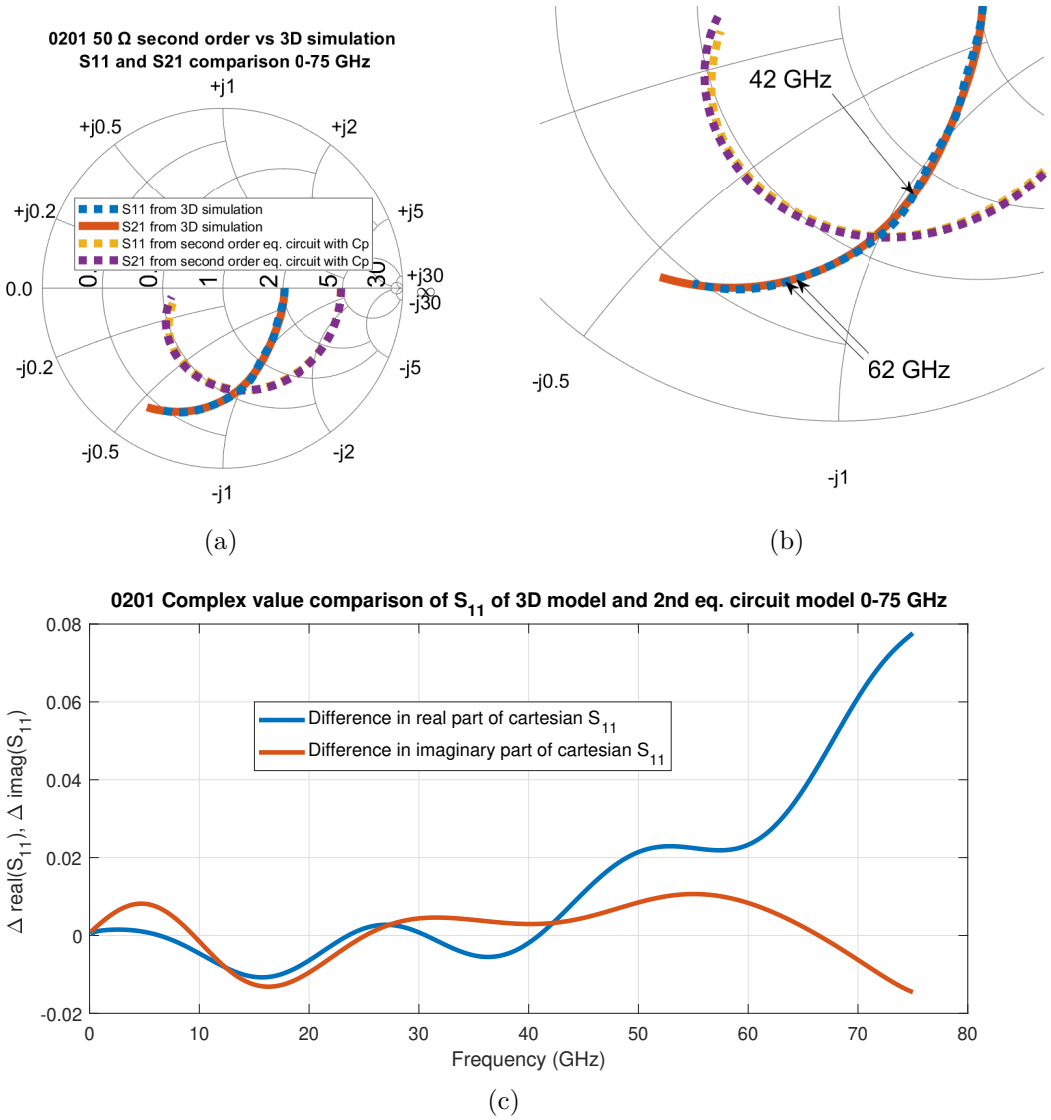

Figure 4.8: (a) A comparison of the S_{11}-parameters from a 3D simulation and a second order equivalent circuit. The S_{11}-parameters from the 3D simulation was used to extract the values of the components in the equivalent circuit. (b) zoomed in version of (a) which highlight how synced both models are at frequencies beyond 42 GHz. (c) A real and imaginary part value comparison between the two simulations.

4.2.2 Extraction of parameters using the model without a shunt capacitor.

4.2.2.1 0402 Parameters

Equations 2.10 - 2.12 were used to calculate the Y-parameters. Y_1, Y_2 and Y_3 was then identified as an capacitor, capacitor and inductor respectively. By plotting L, C_g1 and C_g2 curves as seen in figure 4.9, linear fitting can be performed to extract these individual values that will be used in the equivalent circuit model seen in figure 2.8.
The values gathered from the linear fitting of the curves are

$$L = 0.438 \text{ nH}$$
$$C_g1 = 0.0465 \text{ pF}$$
$$C_g2 = 0.0459 \text{ pF}$$

The extrinsic parameters remain the same as for the previous equivalent model.

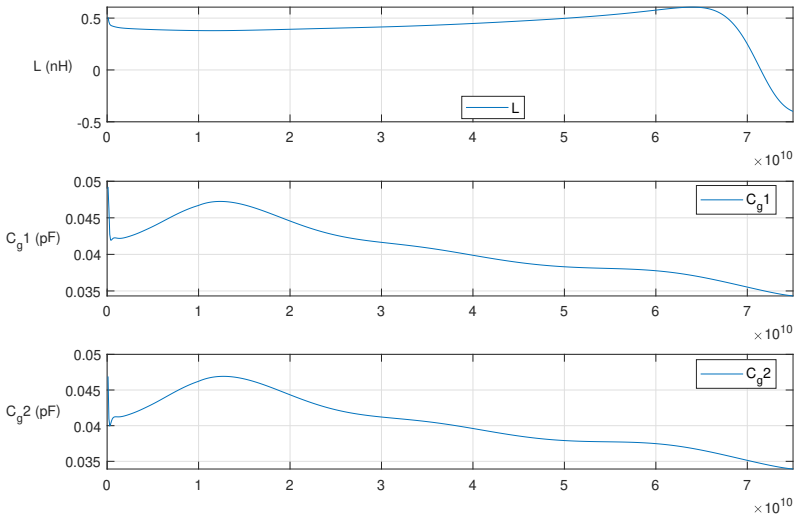

Figure 4.9: Curves of L C_g1 and C_g2 that was extracted from S-parameters.

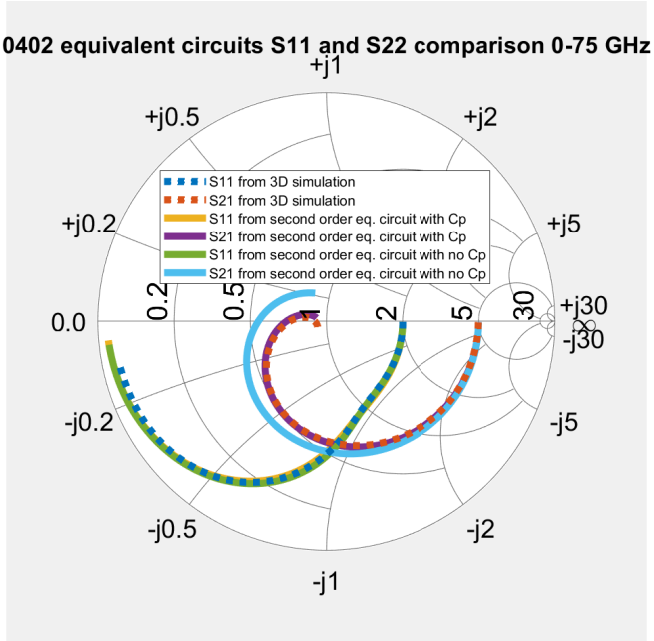

Figure 4.10: Comparison of S_{11}, S_{21} of two different 0402 equivalent circuit models. A difference in S_{21} is more clear than a difference in S_{11}.

4.2.2.2 0201 Parameters

Using the very same methods as for the 0402 parameters, figure 4.11 shows the achieved results using the two different equivalent circuits models.

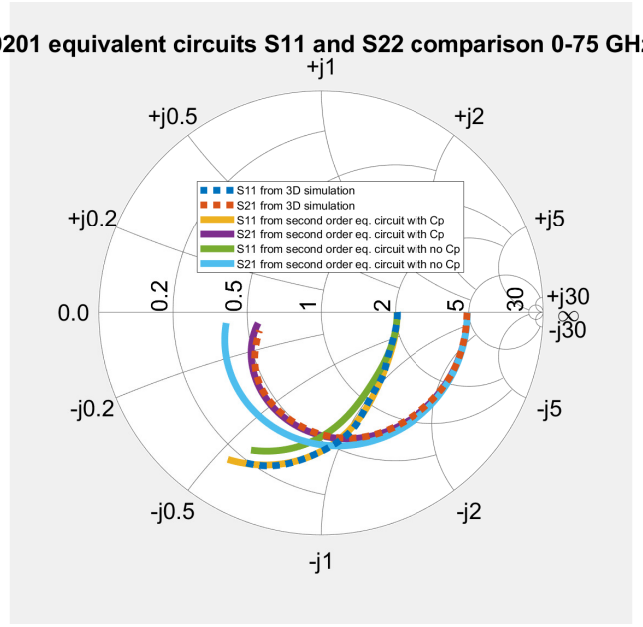

Figure 4.11: Comparison of S_{11}, S_{21} of two different 0201 equivalent circuit models.

4.2.3 Comparison of models for 0402 and 0201 resistors

A comparison between the the first and second order and a 3D model in Ansys is shown in figure 4.12 and 4.13 which are the 0402 and 0201 models respectively. A better similarity is achieved when the pads are considered in form of added transmission lines to the equivalent circuit model.

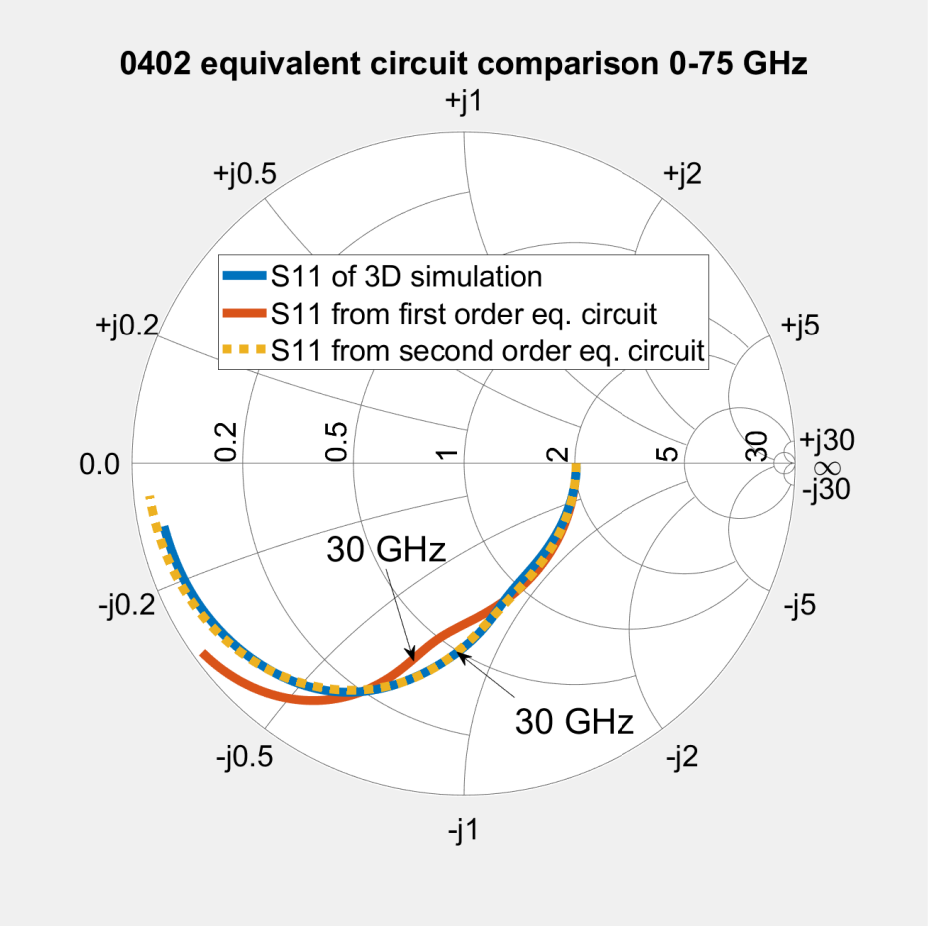

Figure 4.12: A Smith chart presentation of the S_{11} parameters of three models of a 0402 resistor. The blue trace is the 3D simulated and therefore the most accurate model of a resistor. Note the improvement between the yellow and red traces in similarity to the blue trace. The yellow trace represents the second order equivalent circuit model with added transmission lines.

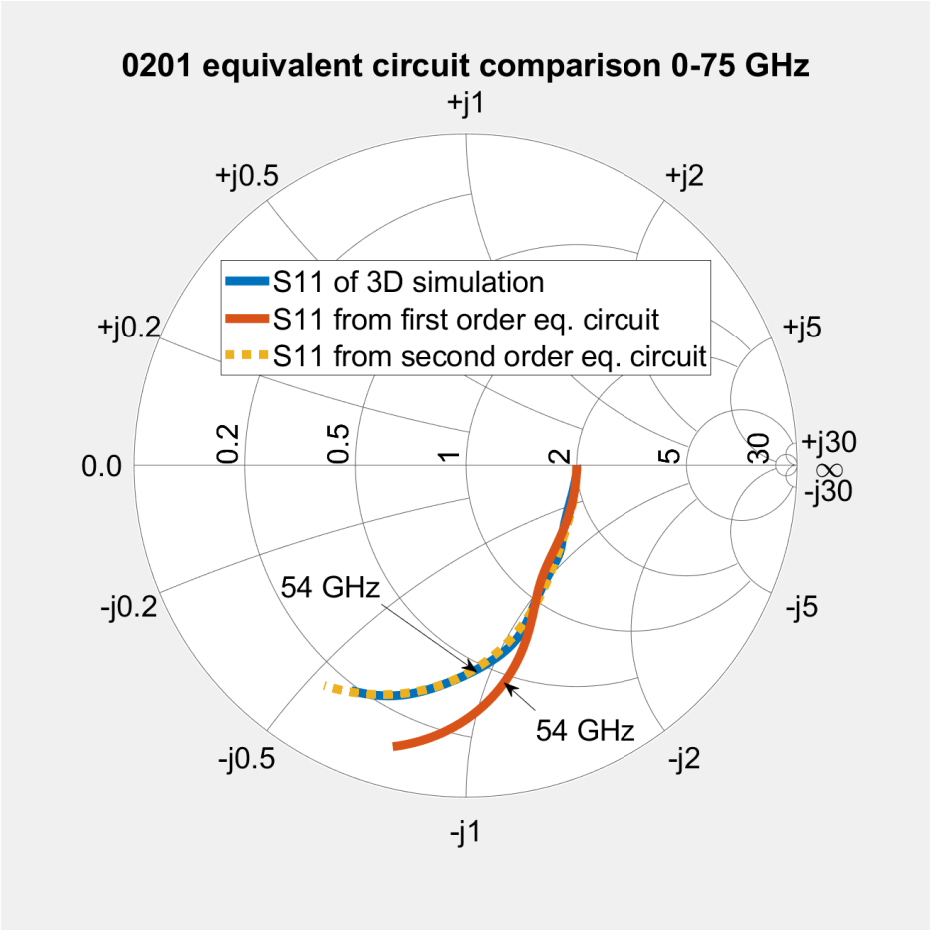

Figure 4.13: A Smith chart presentation of the S_{11} parameters of three models of a 0201 resistor. The blue trace is the 3D simulated and therefore the most accurate model of a resistor. A big improvement can again be observed as previously done with the 0402 model. The yellow trace represents the second order equivalent circuit model with added transmission lines.

4.3 Scalable circuit model

In the final step of modeling, the equivalent circuit is designed to be scalable with resistance, substrate height, and permittivity. This section presents the results within the following limited range:

Scalable ranges of the resistor model	
Parameter	**Range**
Resistance (Ohm)	42 - 112
H_{sub} (mil) / ε_r	0.94 - 5
H_{sub} (mil)	4.7 - 13
Permittivity ε_r	2.6 - 5

Table 4.1: Scalable ranges that will be presented in this result section

4.3.1 Scaling with resistance

Results for resistances below 42 and above 112 ohms, found by optimizing intrinsic parameters and adjusting circuit topology, are excluded to maintain consistency with the derived equations, as explained in the method section. The presented plots of the parasitics are all extracted from equation 2.7-2.8 with simulation setups using $H_{sub} = 7.874$ mil and $\varepsilon_r = 3.3$.

In figure 4.14 the film inductance L is shown as a function of resistance. The decaying inductance is expected from equation 2.7 as $-R^2$ grows faster than $R/Re(Y_{11})$.

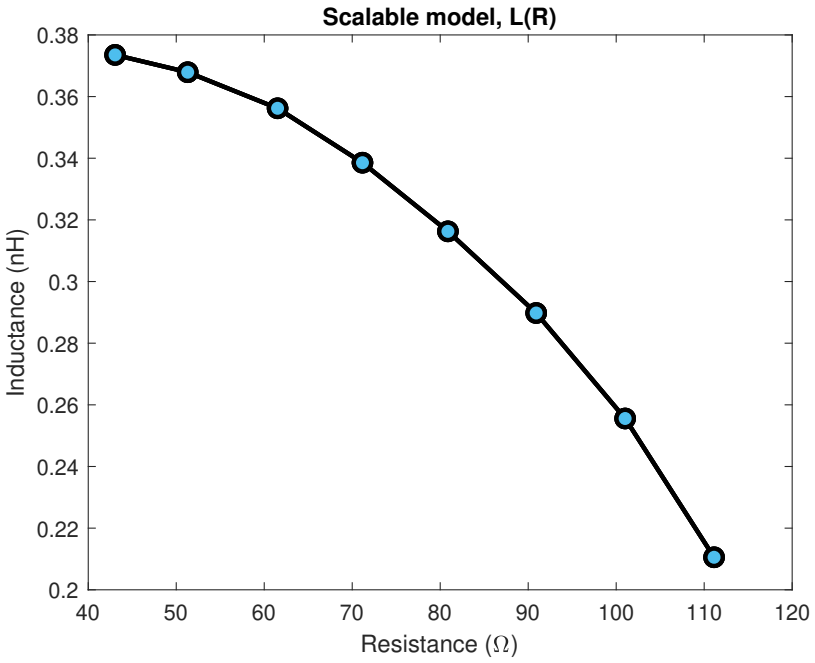

Figure 4.14: Parasitic inductance as a function of resistance in the specified range

The capacitance between the the pads and terminals C_P exhibits similar behavior as the film inductance. This behaviour is in line with equation 2.8, which indicates that as R becomes very large, the first term in the expression tends towards zero. Consequently, $-Im(Y_{11})$ becomes the dominant term.

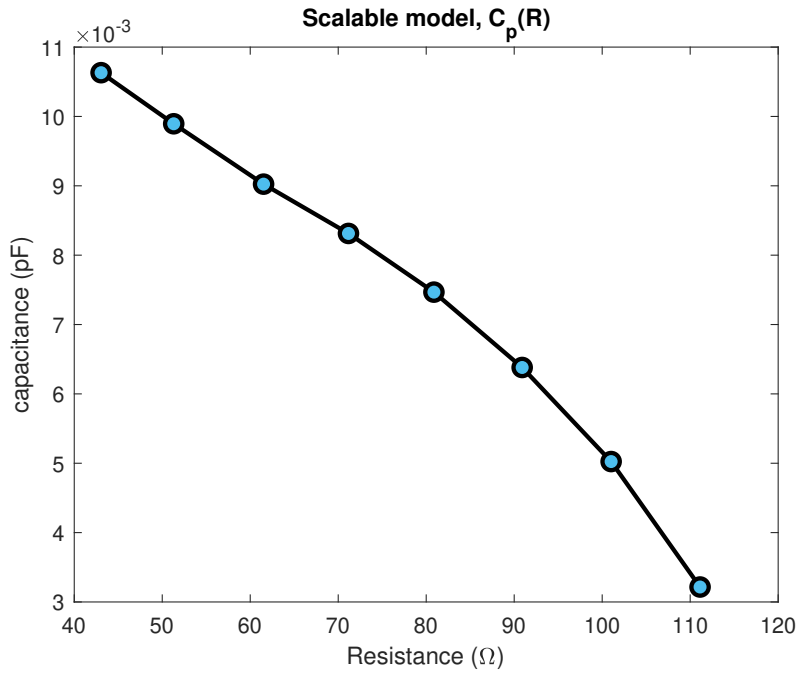

Figure 4.15: Parasitic capacitance C_p as a function of resistance in the specified range

The last intrinsic parameter, C_g, might initially seem arbitrary, However the fluctuations along the y-axis are insignificant, allowing for a mean value of 0.0295 pF to be established. The variance between the minimum C_g at 70 ohms and the maximum at 50 ohms is less than 1%. In Equation 2.9, one notices a dependence on C_p and L, albeit these dependencies are markedly smaller compared to other terms in the expression. This observation suggests that C_g does not necessarily need to scale with R.

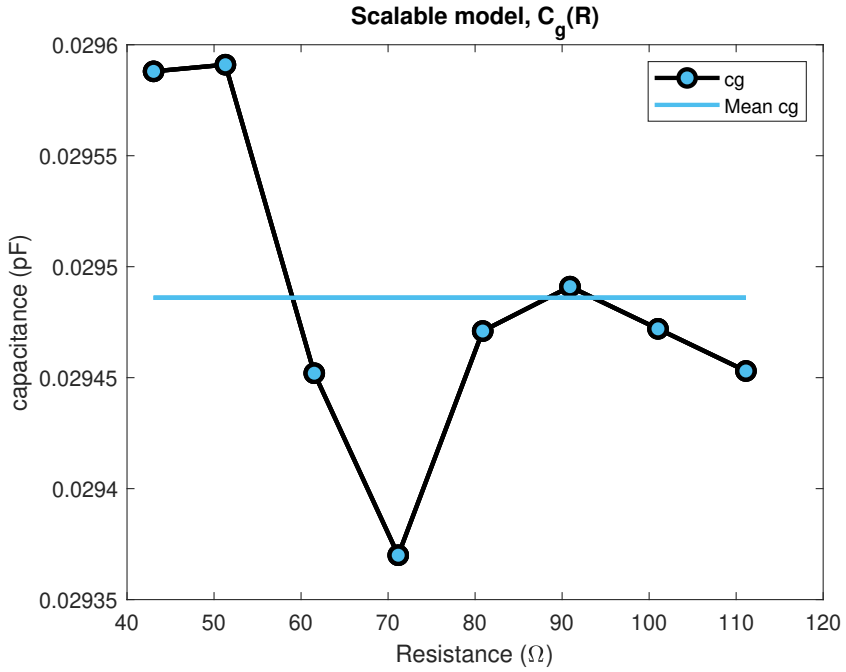

Figure 4.16: Parasitic C_g as a function of resistance in the specified range

4.3.2 Scaling with substrate properties

Table 3.2 showed the simulations that were used to investigate how the substrate properties affects both intrinsic and extrinsic parameters. In this subsection, the substrate impact on extrinsic parameters will first be presented, followed by the intrinsic ones.

From Figure 4.17, it is evident that L_{TML} is dependent on H_{sub}, with no noticeable impact from ε_r. The linear relationship ceases at a ratio of 3.27, corresponding to a permittivity of 2.39, as indicated in Table 3.2. On the other hand, C_{TML} follows the behavior expected of a parallel plate capacitor: $C_{\mathrm{TML}} \propto \frac{\varepsilon_r}{h}$. Decreasing permittivity decreases capacitance, and increasing substrate height decreases capacitance, as illustrated in the lower plot. Within the ratio range of 2-3.3, the proportionality holds nearly perfectly; decreasing ε_r by a factor x and increasing H_{sub} by the same factor yields identical output values. However, outside this range, the relationship becomes increasingly nonlinear. Therefore, an average of both cases are taken to minimize the potential error. Although 4.2.1.1 demonstrated that equation 2.5 and 2.6 could be used to extract the extrinsic parameters with very good accuracy, some fine-tuning was performed to further improve the alignment with the 3D model.

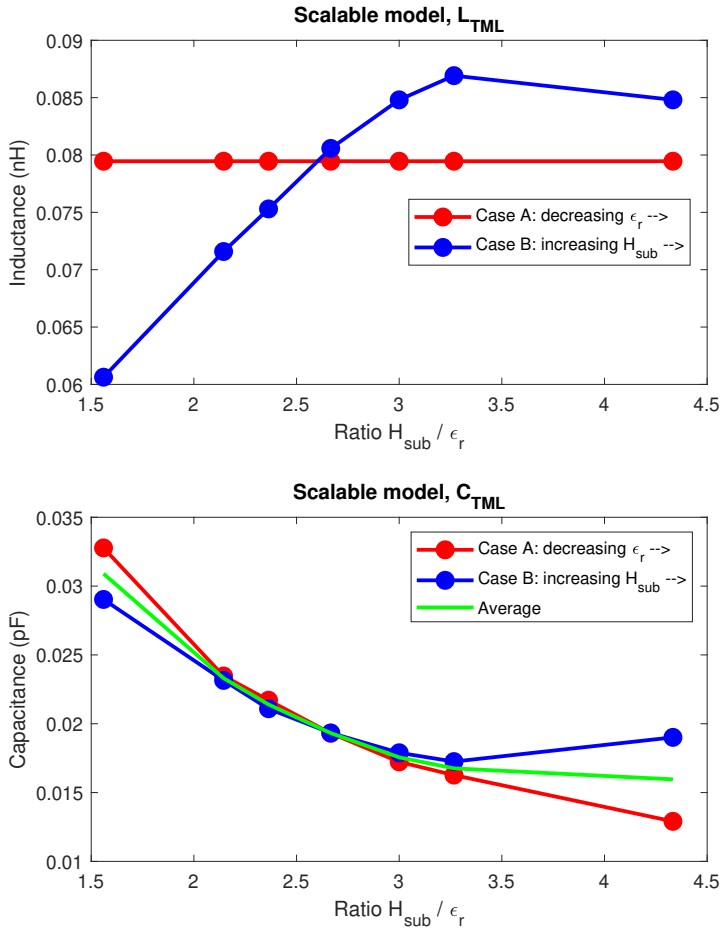

Figure 4.17: Extrinsic parameters as a function of the ratio H_{sub}/ε_r

Unlike the extrinsic parameters, the three intrinsic parameters could be extracted from the derived equations 2.7-2.9 without any fine-tuning.
The capacitance C_g is a similar parasitic to C_{TML}, though they are measured and extracted at different reference planes. Therefore, while they are not identical, they are very similar, especially at lower ratios. Conversely, C_p increases with rising ε_r. A change in the substrate permittivity alters the effective permittivity between the metal terminals. However, C_p requires a larger change in ε_r to be affected in the same way as C_g, because $\varepsilon_{\text{air}} = 1 < \varepsilon_e < \varepsilon_r$. This parasitic also exhibits a slight increase with rising H_{sub}. Between the lowest and highest ratio, its value increases by 8%. The exact reason for this increase is unknown. However, despite the 8% change, its significance is diminished. This is due to the relationship $C_g \approx 3 \cdot C_p$ over the observed range. Consequently, C_g emerges as the dominant capacitor due to its lower cutoff frequency.

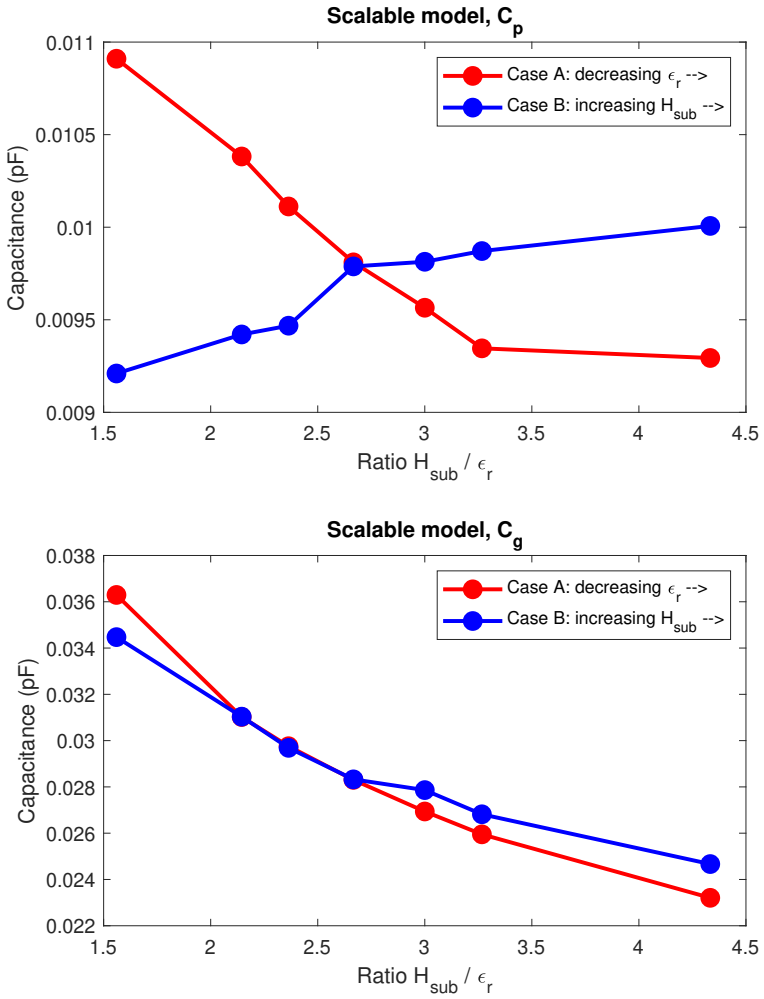

Figure 4.18: Intrinsic capacitances as a function of the ratio H_{sub}/ε_r

The last circuit component to examine is the film inductance L which is presented in figure 4.19. The sweep of H_{sub} in case B shows a negligible variation in the y-axis and are hence considered insignificant while case A shows that ε_r has an impact on the inductance. A decrease in permittivity, decreases the film inductance. This change is not that significant but still noticeable.

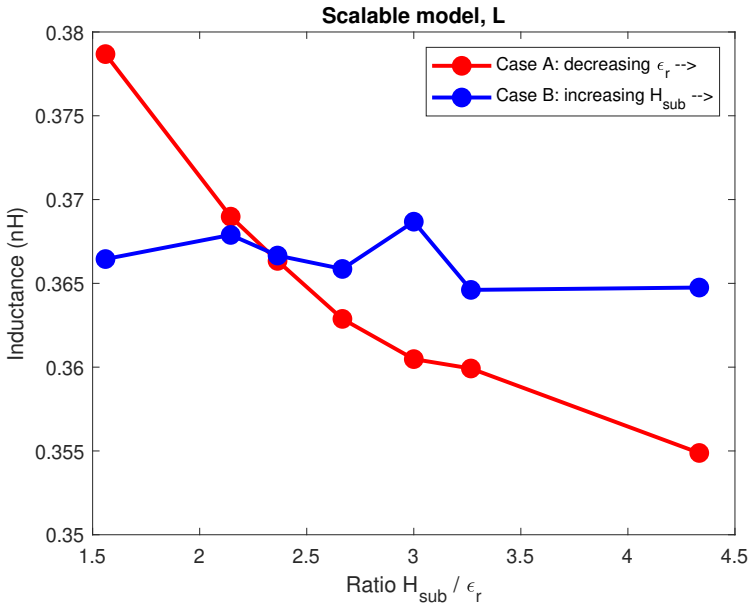

Figure 4.19: Intrinsic inductance as a function of the ratio H_{sub}/ε_r

4.3.3 Compiling and summarizing the scalable model

Now all components in the equivalent circuit presented in 2.7 has been examined with desired scaling parameters. The following summary can be made:

- **Interpolated equations:** All scaling equations have been formulated by creating suitable basic fitting equations that effectively link the extracted discrete data points with a smooth, continuous curve. These curves vary in form between linear, quadratic, and cubic polynomials based on the complexity of the pattern. Interpolation has thus been made between the points.
- **Resistance dependence:** The intrinsic parameters C_p and L depend on the component resistance R, and have been compiled within the 41-111 Ohms interval, allowing the user to scale the component with R. Conversely, intrinsic C_g is independent of R.
- **Proportionality dependence:** Ground capacitances C_g and C_{TML} are scaled with the factor H_{sub}/ε_r.
- **Permittivity dependence:** While C_p and L were shown to be dependent on R, they are also dependent on ε_r which gives an additional scale factor to these two components.
- **Substrate height dependence:** L_{TML} is only scaled with H_{sub} since it is independent of ε_r and R.
- The following scaling ranges should be considered:
  - A spanning of 1-500 Ohms has been examined; ranges beyond 41-111 Ohms were not presented due to reliance on a more empirical methodology.
  - ε_r was found accurate between 2.6 - 5 and H_{sub} between 4.68 mil - 13 mil. Outside these conditions, the model was not tested as it is considered uninteresting configurations for the project.

4.3.4 Verifying the scalable equivalent circuit model with a practical example

As intended, a T-attenuator was designed to validate the applicability of the model in practical circuits. Initially, the attenuator was constructed at the circuit schematic level utilizing three scalable resistors. An optimization objective was established to attain a reflection coefficient (S_{11}) exceeding -10 dB and an attenuation coefficient (S_{21}) equal to -3 dB within the frequency range of 15 to 20 GHz. Upon optimization, with some adjustments, the configuration in table 4.2 was found to fulfill the specified criteria.

3 dB Attenuator configuration	
Parameter	**Value**
$R1, R3$	1 Ohm
$R2$	45 Ohm
H_{sub}	7 mil
Permittivity ε_r	3.4

Table 4.2: Resistor and substrate parameters that satisfies the performance of the desired T-attenuator. Values were found from simple optimization and tuning. R_1 and R_3 are the resistors in series with the line, R_2 is the resistor connected to ground.

The circuit results must be compared to a 3D EM-model in order to verify the credibility of the model. The obtained substrate and resistor values were therefore put into the developed 3D EM-model in the following setup.

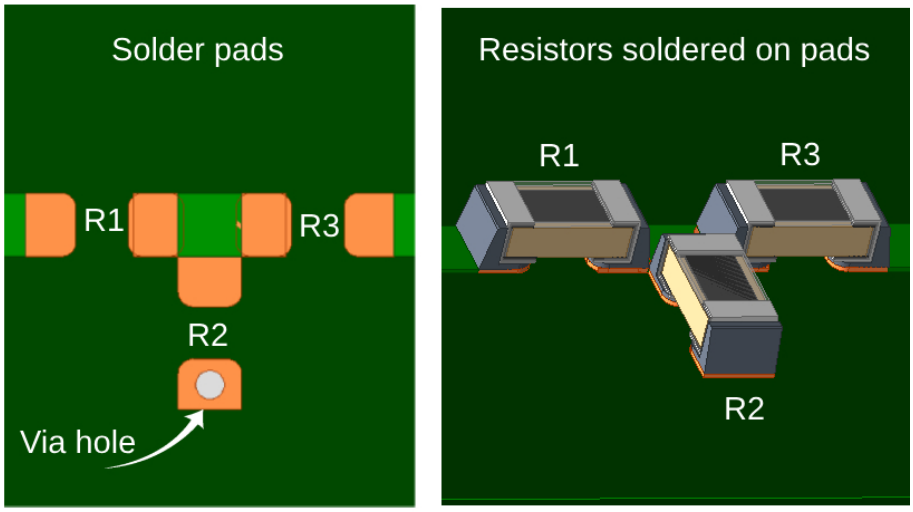

Figure 4.20: Left picture shows the configuration of the solder pads which are identical to the ones used when extracting the scalable model. Right pictures shows the same environment with soldered resistors attached to the pads.

Figure 4.21 shows that the circuit attenuation $S_{21,circuit}$ and 3D attenuation $S_{21,3D}$ are almost identical. It also shows that the circuit reflection $S_{11,circuit}$ and 3D reflection $S_{11,3D}$ are very similar, but there is a noticable difference. At 20 GHz, the difference in the reflection coefficient is $\Delta S_{20\text{ GHz}} = 0.84\,\text{dB}$, and at 15 GHz, it is $\Delta S_{15\text{ GHz}} = 1.35\,\text{dB}$.

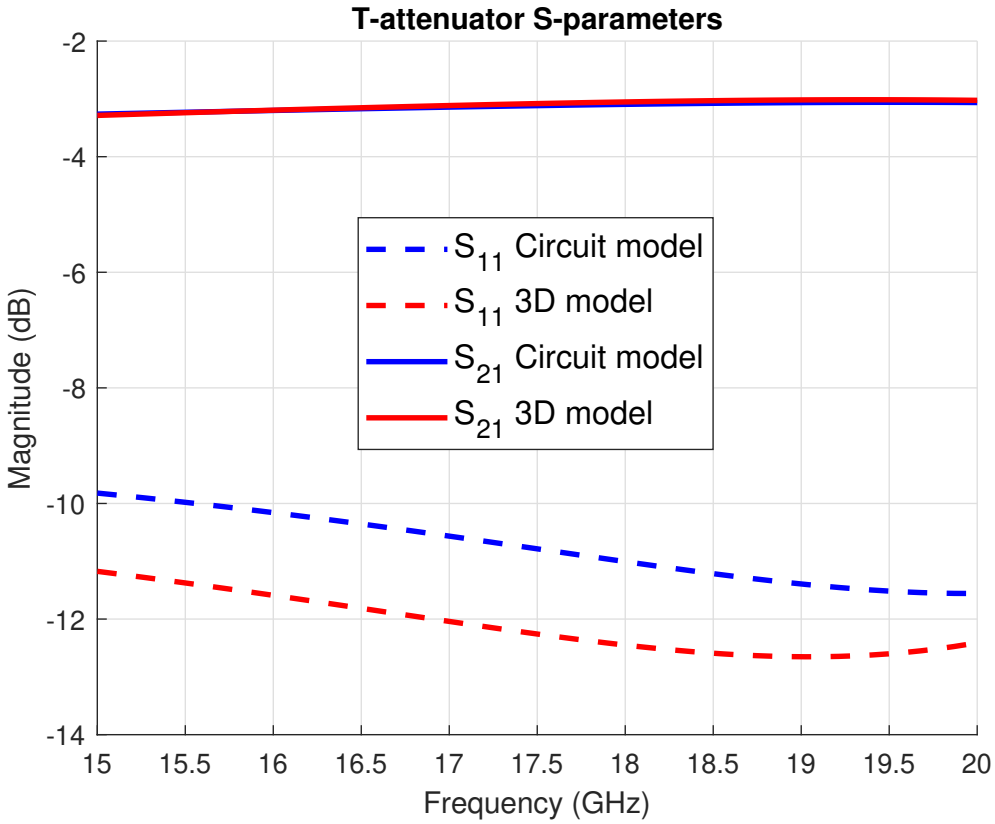

Figure 4.21: 3 dB T-attenuator results when comparing the equivalent scalable circuit model with the 3D model

To better understand the differences in S-parameters, it is necessary to analyze the S-parameters over a broader frequency band and on the Smith chart. Figure 4.22 shows that there is a small frequency shift at the resonance frequency for s11 where $\Delta S_{32.2\ \mathrm{GHz}} = 0.21\,\mathrm{dB}$. A far more accurate value than the values in the desired band. Although the reflection is slightly shifted, the scalable equivalent circuit model is still able to catch the same behaviour and pattern as the 3D model.

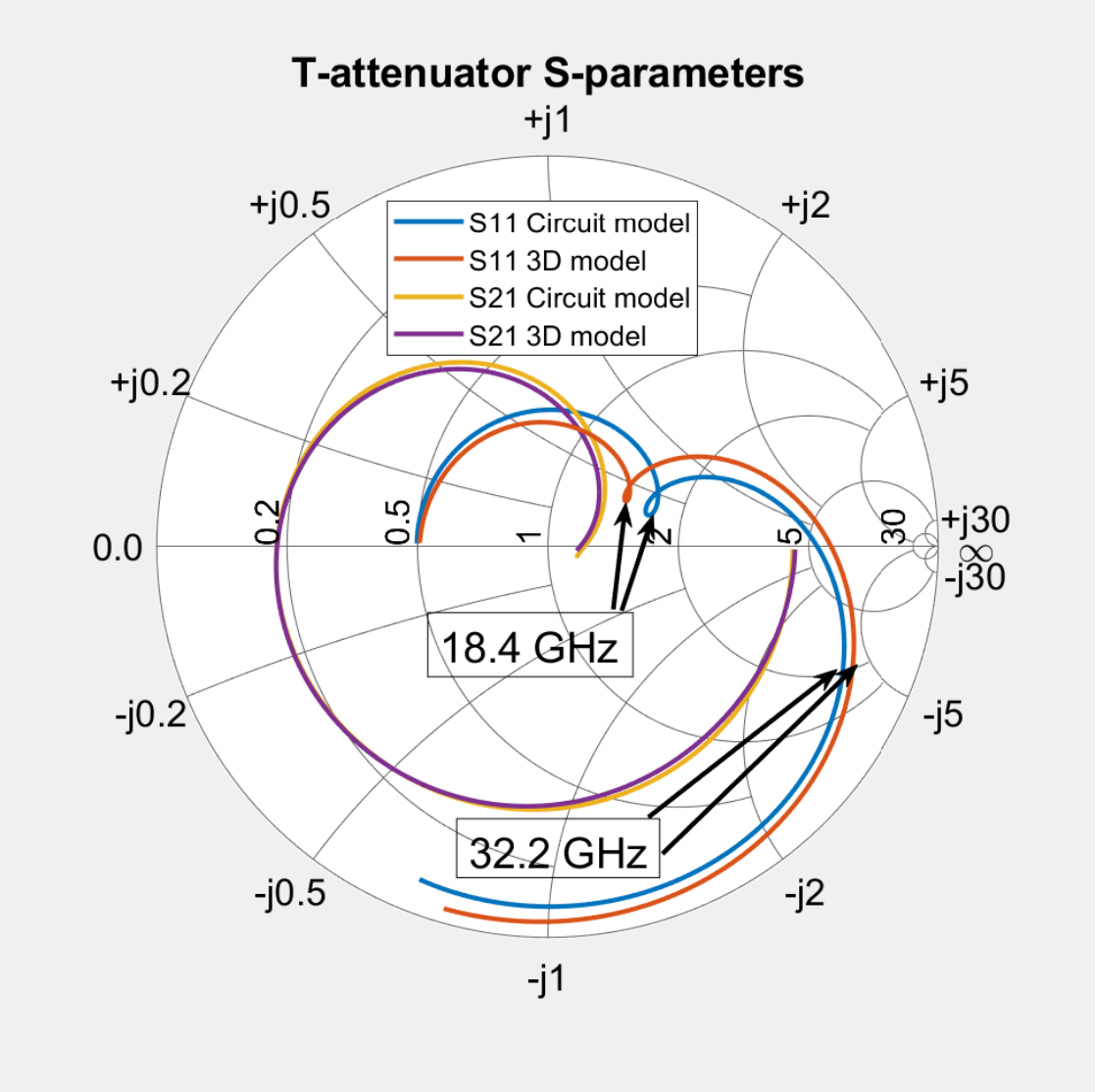

Figure 4.22: T-attenuator Circuit model vs 3D model in 0.1-50 GHz. Arrows pointing at 18.4 GHz and 32.2 GHz respectively, visualizing the performance difference at the resonance frequency compared to a random frequency in the band.

5
Discussion

This thesis project has successfully developed 3D models and scalable equivalent circuit models of SMD resistors of the size 0402 and 0201. This chapter delves into the methodological achievements, challenges faced, and propose potential enhancements and directions for future research within SMD resistor modeling.

5.1 3D model: Examining parameters that potentially affects the parasitic effects.

The initial goals was to develop a 3D model which captures parasitic behaviour that arises and increases with frequency. It was reported that it is usually the resistive film that is protected by IP from the component manufacturers while the exterior part is commonly exposed in the datasheet. Therefore the film dimensions were explored which showed that the only unknown parameter that may affect the parasitics are the film width. Figure 4.4 shows that a more narrow film results in a larger "radius" of the parasitic behaviour which is equivalent to an increase in parasitic inductance. This phenomenon aligns with established microwave literature, which highlights the inherently inductive nature of narrow traces. Despite variations in film widths, the deviations are minimal, allowing for reasonably accurate assumptions. To refine these assumptions, three randomly selected SMD resistors underwent X-ray analysis, indicating that a film width occupying 75% of the SMD width is plausible. The thickness was arbitrarily assumed to be 12 micrometers, as thickness has been shown not to significantly affect parasitics, as seen in Figure 4.6.

5.1.1 Evaluating the Accuracy of the 3D Model: Simulation vs. Experiment

To validate the 3D model constructed in HFSS, along with the film width assumption, a measurement of a 47 Ohm SMD resistor was conducted. Due to calibration limitations on the Ikaros PCB, measurements were restricted to frequencies up to 32 GHz, demonstrating almost identical behavior to the 3D model, as depicted in Figure 4.2. It is presumed that this resemblance in behavior persists as the frequency surpasses 32 GHz. Differences were visible in the comparison, these are credited due to TRL calibration uncertainties that occurs at the start and end of the chosen frequency range as explained in the method section. The decision to trust the 3D model more than the real resistor was made. A very important step in creating a

3D model is to ensure that the model being created is as identical as possible to the real component. Nevertheless, the method outlined herein demonstrates that this task can be achieved with good precision. For additional validation, it would be preferable to verify the model using other resistance values. However, during the project, only a 47-ohm resistor was available.

5.2 Comparing with other models

Two different equivalent circuits were created for non EM simulation based software that allows scalability, optimization and time saving. It was important that these models were as identical to the 3D model as possible which is why — while creating these models — comparisons with the 3D simulations were constantly made to ensure the validity. Both equivalent circuit models (with and without a shunt capacitor C_p, the one without is based on the paper found here [12]) had very identical S_{11}-parameters when compared to 3D simulations but the model without a shunt capacitor did not replicate the resulting S_{21}-parameter, instead it showed less loss than it should. This lack of loss is due to the impedance presented by the capacitance C_p. The model with a parasitic capacitor C_p and indistinguishable capacitors C_g was therefore the most identical model when compared to the 3D model. Excluding this component logically leads to inaccuracies at high frequencies because a capacitor acts as a short circuit at those frequencies. Without the capacitor, the model wronlgy allows a larger portion of the signal to pass through the inductor, causing S_{21} to deviate from the 3D simulation. However, this issue is bypassed at low frequencies since the capacitor is treated as an open circuit.
It is also very important that the transmission lines are accounted for as seen in figure 4.12, 4.13. This project utilizes a π-network consisting of two capacitors and a inductor which will work as an approximation of a transmission line. The derived expression holds true, mathematically as long as $\beta \mathrm{l} << 1$.

Comparing the second order equivalent circuit with the 3D simulations shows a success in the goal to capture the parasitics and will thus save the user of having to perform 3D simulations when using the resistor. As stressed by Modelithics, it is however important to perform 3D simulations to capture coupling effects when the resistor is in an environment with other components.

5.3 Developing a scalable equivalent circuit model

A scalable equivalent circuit model has been successfully developed and demonstrated. The method involved extracting parasitic parameters at different values of R, H_{sub}, and ε_r. Fitting equations were created between discrete points, indicating that some variables depend on more than one scaling equation. For example, C_p was shown to be dependent on R, as expected from the derived equations but also ε_r, as the substrate permittivity affects the effective permittivity between the solder pads and metal terminals of the resistor.

Although the equivalent circuit was developed to closely match the 3D model, the scalable model is expected to exhibit larger non-negligible uncertainties. This is due to the reliance on interpolated fitting equations, which can introduce minor errors that accumulate and affect overall accuracy. The complexity of interpolation and inherent imperfections in the model mean that different configurations may vary in accuracy. This is particularly true when multiple resistors are included in the model, as errors can multiply. For instance, if the scalable model has an error of x for a certain input, simulating three resistors simultaneously could result in a total error of $3x$.

Another challenge is to generalize the model's error quantification because different combinations of ε_r, H_{sub}, and R can vary in magnitude. For example, the random optimized combination for the T-attenuator showed a maximum error of $\Delta S = 1.35\,\text{dB}$ at 15 GHz in the 0-42 GHz band. However, this is acceptable as the equivalent circuit model is intended as a preliminary step in the design stage for microwave designers. Once a configuration meets the desired goals, it should be verified with 3D EM models. If the EM simulation does not meet the goals, only minor adjustments are necessary to achieve the final result. Starting with the 3D model would be more complex and time-consuming, requiring numerous iterations to achieve the same results. In this particular T-attenuator example both circuit and 3D model satisfied the results, with only 1 required EM iteration. Other configurations might yield higher or lower uncertainties depending on the combination, potentially requiring more than 1 iteration to satisfy the results with the EM-model. Most likely another random configuration should be more accurate since this example involved two 1 Ohm resistors which are already pushing the limits of the model.

6
Conclusion

A scalable equivalent circuit model and a 3D model, both compatible with substrate properties and device resistance, have been successfully developed for the frequency range of 0-42 GHz, applicable to both 0402 and 0201 SMD resistors. An investigation into key parameters identified the film width as the primary geometrical uncertainty affecting parasitic results. This uncertainty can be minimized by making valid assumptions based on x-ray images. Aside from film placement and dimensions, exterior features of the SMD can typically be determined from the manufacturer datasheet or reasonably assumed.

By integrating the developed 3D model with a sophisticated setup in full-wave EM software, a strong correlation between measurements and simulations was achieved, as demonstrated with VNA measurements of an SMD resistor in the 2-35 GHz range. Given its accuracy, it can be used to easily and quickly simulate S-parameters which are used to extract parasitic reactances for an equivalent circuit model. A suitable equivalent circuit topology has been established, with derived equations for each component enabling the extraction of their values. The equivalent circuit model exhibited high accuracy, with minor errors observed between simulation and circuit. Furthermore, the equivalent circuit model was made scalable, allowing for input variations within the reported ranges: resistance between 41-111 Ohms, permittivity between 2.6-5, and substrate thickness between 4.68 mil and 13 mil. Although the model was created for a broader range of 1-500 Ohms, results outside 41-111 Ohms were excluded due to the need for modifications beyond the presented theory and method. The scalable model introduces larger errors than the non-scalable model due to the accumulation of minor errors from several interpolated scaling functions, particularly when simulating multiple resistors simultaneously.

The scalable model was validated against the 3D model using a practical example of a T-attenuator. It was demonstrated that a 3 dB T-attenuator with a reflection coefficient better than -10 dB between 15-20 GHz can be designed by placing three resistors in a T-configuration, setting up requirement goals, and running an optimization. While the 3D EM model revealed small but noticeable differences, the EM simulation satisfied the result using the optimized configuration without any fine-tuning.

In conclusion, the developed models enable microwave engineers to design and verify practical circuits involving the examined SMD resistors efficiently, without needing to address the complexities detailed in this report.

The project's purpose and goals have been successfully achieved. It is likely that a significant portion of the established results can be applied to other SMD components, such as capacitors and inductors. While the intrinsic circuit topology may require minor adjustments, the extrinsic topology can remain identical since it represents a solder pad. The primary challenge with inductors and capacitors lies in understanding the more complex geometry of their 3D components compared to SMD resistors.

Bibliography

[1] Frequency Response of Thin Film Chip Resistors (2023) https://www.vishay.com/docs/49427/vse-tn00.pdf

[2] Nantian Electronics, (2023) Difference Between Thin Film Resistors and Thick Film Resistors https://www.ntchip.com/electronics-news/difference-between-thin-film-resistors-and-thick-film-resistors

[3] Pozar, David M. (2021) Microwave Engineering, Internation Adaptation Chapter 3: Transmission lines and Waveguides.

[4] KOA Corporation (2024) Basics of resistor. https://www.koaglobal.com/product/library/resistor/basic?sc_lang=en

[5] Engen, G.F. and Hoer, C.A. (1979) Thru-Reflect-Line: An Improved Technique for Calibrating the Dual Six-Port Automatic Network Analyzer. 10.1109/TMTT.1979.1129778

[6] Microwave Journal (2020) Moving Beyond S-Parameter Files: Advanced Scalable and 3D EM Models for Passive Devices. https://www.microwavejournal.com/articles/print/33613-moving-beyond-s-parameter-files-advanced-scalable-and-3d-em-models-for-passive-devices

[7] Modelithics (2020) Application Note No.63 Introduction to Modelithics 3D Models in HFSS https://www.modelithics.com/Downloads/AppNotes/AN063_3D_Models_in_HFSS_Final.pdf

[8] EEPOWER (2022) Thin and Thick Film Chapter 4 - Resistor Materials https://eepower.com/resistor-guide/resistor-materials/thin-and-thick-film/#

[9] Krishna Seshan and Dominic Schepis Handbook of Thin Film Deposition (2018)

[10] Michael I. Panzini (2011) Thick Films: Properties, Technology and Applications (Materials Science and Technologies: Electrical Engineering Developments)

[11] David J. Griffiths (2020) Introduction to Electrodynamics Fourth Edition Chapter 7.2 Electromagnetic Induction

[12] J. Chen, X. -M. Li and R. -X. Wu, "Equivalent Circuit Model of Lumped Elements Retrieved from Measured S-Parameters of Microstrip Line in Frequency Range 0.5-5GHz," 2020 IEEE MTT-S International Wireless Symposium (IWS), Shanghai, China, 2020, pp. 1-3, https://doi.org/10.1109/IWS49314.2020.9360005

[13] Ansys, Inc. (2020) Module 6: HFSS Lumped and Wave Port Basics Wave Port Sizing https://courses.ansys.com/wp-content/uploads/2021/07/HFSS_GS_2020R2_EN_LE6_Port_Basics.pdf

[14] UIC AREA, Alyssa Yaeger

[15] EMI Analsyt (2023) Microstrip Inductance https://www.emisoftware.com/calculator/microstrip/
[16] All About Circuits Microstrip Inductance Calculator https://www.allaboutcircuits.com/tools/microstrip-inductance-calculator/
[17] EverythingRF Microstrip Impedance Calculator https://www.everythingrf.com/rf-calculators/microstrip-impedance-calculator

A

Appendix 1

A.1 Derivation of inductor and capacitor in π network approximation of a transmission line

The ABCD matrix of a lossless transmission line is

$$\begin{bmatrix} A & B \\ C & D \end{bmatrix} = \begin{bmatrix} \cos(\beta l) & jZ_0 \sin(\beta l) \\ jY_0 \sin(\beta l) & \cos(\beta l) \end{bmatrix} \tag{A.1}$$

Using a Taylor approximation for $\beta l << 1$

$$\begin{bmatrix} A & B \\ C & D \end{bmatrix} = \begin{bmatrix} 1 - \frac{(\beta l)^2}{2} & jZ_0 \beta l \\ jZ_0 \beta l & 1 - \frac{(\beta l)^2}{2} \end{bmatrix} \tag{A.2}$$

The ABCD matrix of the π network consisting of an inductor and capacitors to ground is given by

$$\begin{bmatrix} A & B \\ C & D \end{bmatrix} = \begin{bmatrix} 1 - \omega^2 L_{TML} C_{TML} & j\omega L_{TML} \\ j\omega C(2 - \omega^2 L_{TML} C_{TML}) & 1 - \omega^2 L_{TML} C_{TML} \end{bmatrix} \tag{A.3}$$

Equating matrix A.2 with matrix A.3 yields $L_{TML} = \frac{Z_0 \beta l}{\omega}$, $C_{TML} = \frac{\beta l}{2\omega Z_0}$

DEPARTMENT OF Microtechnology AND NANOSCIENCE
CHALMERS UNIVERSITY OF TECHNOLOGY
Gothenburg, Sweden
www.chalmers.se